

The role of ventilation in managing moisture inside New Zealand homes

Stephen McNeil, Manfred Plagmann, Peter McDowall and Mark Bassett





1222 Moonshine Rd
RD1, Porirua 5381
Private Bag 50 908
Porirua 5240
New Zealand
branz.nz



**MINISTRY OF BUSINESS,
INNOVATION & EMPLOYMENT**
HĪKINA WHAKATUTUKI

The work reported here was jointly funded by BRANZ from the Building Research Levy, the Ministry of Business, Innovation and Employment and the companies whose logos are shown above.

Acknowledgements

This work was jointly funded by the Building Research Levy and the Ministry of Business, Innovation and Employment. Special mention must also go to Malcom Cunningham, Luca Quaglia and Mikael Boulic for their contributions at the beginning of this project. We would also like to thank Inga Smith for her contributions throughout the project. A number of companies provided support in kind and deserve recognition:

- The Fraunhofer Institute for Building Physics for their continued collaboration with BRANZ on this project and providing access to their WUFI Plus software.
- Tony Sandes on behalf of DVS for providing a DVS ventilation system.
- Hometech for supply of their passive stack ventilators.
- Marshall Innovations for providing their Trade Seal collars.

The role of ventilation in managing moisture inside New Zealand homes

BRANZ Study Report SR341

Author(s)

Stephen McNeil, Manfred Plagmann, Peter McDowall and Mark Bassett

Reference

McNeil, S., Plagmann, M., McDowall, P. and Bassett, M. (2015). *The role of ventilation in managing moisture inside New Zealand homes*. Study Report SR341, BRANZ Ltd, Judgeford.

Abstract

Ventilation, insulation and heating are the key components to ensuring a healthy indoor environment. This work studied airtightness and actual in-service ventilation rates in a variety of modern housing stock. In-service ventilation rates indicated that on average around a third of these homes were under ventilated. The airtightness results were also compared to previous work, indicating a clear trend to more airtight buildings, further work evaluated the consequence of this from the point of view of managing moisture. An experimental facility that had airtightness variable from 1-9 ACH@50Pa was constructed to evaluate ventilation options, at different levels of airtightness. It was shown there was a reduction in how long moisture remained in the air as ventilation was increased, though the effect was tempered by the sorption into building materials, and condensation on surfaces. Our experiments were used to benchmark comprehensive computer models that allow for parametric studies using different input parameters. Finally a field study of supply only ventilation systems was also completed, which gave input into refined control algorithms to minimise the energy impact of ventilation, while in turn maximising their moisture removal efficiency.

Keywords

Ventilation, Infiltration, Airtightness, Tracer gas, Moisture, Moisture removal

Contents

1. INTRODUCTION	1
1.1 Airtightness background	2
1.2 Ventilation and airtightness	3
2. EQUIPMENT	6
2.1 The experimental building	6
2.1.1 Characteristics of the ports	7
2.1.2 Instrumentation	8
2.2 Blower door – whole-house pressurisation	10
3. EXPERIMENTAL METHODS	11
3.1 Airtightness and ventilation survey	11
3.1.1 Selection of houses	11
3.1.2 Airtightness measurement	11
3.1.3 Mean ventilation rate measurement	11
3.2 Experimental building	13
3.2.1 Tracer techniques	13
3.2.2 General mass balance equation	13
3.2.3 Distribution of sampling and dosing points	14
3.2.4 Infiltration experiments – building characteristics	14
3.2.5 Mixing experiments	14
3.2.6 Ventilation and infiltration experiments – two zone	16
3.2.7 Moisture removal effectiveness	17
3.2.8 CONTAM modelling	23
3.2.9 Two-zone ventilation and infiltration model	23
3.3 Control system evaluation	24
3.3.1 WUFI Plus modelling	25
4. RESULTS.....	27
4.1 Ventilation and airtightness survey	27
4.2 Infiltration measurement	29
4.3 Tracer gas mixing experiments	31
4.3.1 Vertical mixing	31
4.3.2 Horizontal mixing	31
4.4 Ventilation measurements – two zone	34
4.5 CONTAM modelling	37
4.5.1 Single-zone infiltration model	37
4.5.2 Infiltration in different cities	40
4.5.3 Two-zone infiltration and ventilation model	47
4.6 Moisture removal effectiveness	48
4.6.1 Rode model	49
4.6.2 Nodal model	50
4.7 Control system evaluation	52
4.7.1 Empirical measurement summary	52
4.7.2 WUFI Plus modelling summary	52
5. SUMMARY	56
REFERENCES	58

Figures

Figure 1. Summary of earlier airtightness in New Zealand.....	1
Figure 2. Estimated infiltration and measured ventilation. The green band indicates the range of acceptable ventilation rates in countries where there is a minimum rate defined. Note that flow rates are given as air changes per hour at atmospheric pressure.....	4
Figure 3. a) Photograph of the experimental building on site. b) Basic floor plan of the test building.	6
Figure 4. Measured data and fitted function for the flow characteristic of the various ports.....	7
Figure 5. Instrumentation scheme used in the house.	8
Figure 6. Pressure-averaging tube schematic. P_H and P_L represent the average impact and static pressures respectively. Adding them gives DP , which can be correlated to flow in the tube.	9
Figure 7. Typical distribution of tracer sources and sampling tubes (sources in red, samplers in blue).	12
Figure 8. Locations of the sampling and dosing points in Zones 1 and 2 for horizontal mixing experiments. All sampling points were at a height of 1600 mm from the floor. Distances indicated in the figure are in units of mm.....	15
Figure 9. Building floor plan showing Zone 2 as the smaller bedroom.	16
Figure 10. Two-zone ventilation – supply-only roofspace system.	16
Figure 11. Nodes in building components describe the building as a physical system.....	20
Figure 12. Section of the graphical representation of a nodal model with an edge property overlay.	21
Figure 13. CONTAM two-zone model floor plan – 1 ACH @ 50Pa case shown.	24
Figure 14. Sensor layout in Dunedin homes – red and blue dots indicate temperature and humidity sensors respectively.	25
Figure 15. Distribution of airtightness measurements for post-1994 homes.	27
Figure 16. Distribution of airtightness results, with specific ventilation and obvious leakage openings sealed.....	27
Figure 17. Infiltration versus measured ventilation, with outliers circled. Note that flow rates are given as air changes per hour at atmospheric pressure.....	28
Figure 18. Single-zone infiltration rate of the living area at different N_{50} airtightness levels. The graph for the airtightness level of 9 ACH is provided separately due to its increased scale (see Figure 19.).....	29
Figure 19. The graph shows the single-zone infiltration rate of the living area at about 9 N_{50} . All ports are open at this level of airtightness, but windows and doors are closed.	30
Figure 20. Infiltration rates for the two zones described in Figure 9. The legend shows the direction of flow (Q) for each line, where Zone 1 is denoted by the subscript 1, Zone 2 is denoted by subscript 2 and outside is denoted by subscript 0.	30
Figure 21. Results of vertical mixing experiment for Zones 1 and 2. Three sample points were used – 2065 mm (top), 1065 mm (middle) and 55 mm (bottom) above the zone floor. The two uppermost plots show the difference in SF_6 concentration between the top sample point and the middle and bottom sample points.	31

Figure 22. Results of horizontal mixing experiment for Zones 1 and 2. Four sampling points were used in each zone as illustrated in Figure 8. A consistent SF₆ concentration across all sampling points in Zone 1 indicates good mixing in the horizontal plane within that zone. Variation in tracer gas concentration at different sampling points in Zone 2 suggests incomplete mixing within that zone. 32

Figure 23. Mean total ventilation rates for each zone versus airtightness – infiltration only. 34

Figure 24. Mean ventilation rates for each zone versus airtightness – supply-only ventilation. 35

Figure 25. Interzonal ventilation rates for each zone versus airtightness – infiltration only – year 1. 35

Figure 26. Infiltration only – year 2. 36

Figure 27. Ventilation rate with supply-only ventilation – year 2. 36

Figure 28. (a) Yellow dots = empirical measurement of the infiltration rate for the experimental test building at 1 ACH @ 50 Pa. Blue solid line = infiltration rate of experimental building determined using CONTAM simulation and a convolution. (b) Graphical representation of CONTAM model used to simulate the infiltration in (a). 38

Figure 29. (a) Yellow dots = empirical measurement of the infiltration rate for the experimental test building at 3 ACH @ 50 Pa. Blue solid line = infiltration rate of experimental building determined using CONTAM simulation and a convolution. (b) Graphical representation of CONTAM model used to simulate the infiltration in (a). 39

Figure 30. (a) Yellow dots = empirical measurement of the infiltration rate for the experimental test building at 5 ACH @ 50 Pa. Blue solid line = infiltration rate of experimental building determined using CONTAM simulation. (b) Graphical representation of CONTAM model used to simulate the infiltration in (a). 39

Figure 31. (a) Yellow dots = empirical measurement of the infiltration rate for the experimental test building at 9 ACH @ 50 Pa. Blue solid line = infiltration rate of experimental building determined using CONTAM simulation. (b) Graphical representation of CONTAM model used to simulate the infiltration in (a). 40

Figure 32. Infiltration model for a single-zone Northland house at various airtightness levels. 41

Figure 33. Infiltration model for a single-zone Auckland house at various airtightness levels. 42

Figure 34. Infiltration model for a single-zone Taupo house at various airtightness levels. 43

Figure 35. Infiltration model for a single-zone Wellington house at various airtightness levels. 44

Figure 36. Infiltration model for a single-zone Christchurch house at various airtightness levels. 45

Figure 37. Infiltration model for a single-zone Dunedin house at various airtightness levels. 46

Figure 38. Mean measured and modelled air change rate in Zone 2 over a range of airtightness levels with supply-only ventilation. 47

Figure 39. Mean measured and modelled air change rate in Zone 2 over a range of airtightness levels – infiltration only. 48

Figure 40. Measured and modelled humidity ratio, 3 ACH @ 50 Pa – supply only. 49

Figure 41. Measured and modelled humidity ratio, 1 ACH @ 50 Pa – infiltration only. 50

Figure 42. Relative humidity and condensation curves for infiltration-only case. Red line = measured relative humidity in the centre of the room. Blue line = model fit of relative humidity. Green line = amount of condensation on the window given by the right-hand axis. 51

Figure 43. Relative humidity and condensation curves with ventilation system on. Red line = measured relative humidity in the centre of the room. Blue line = model fit of relative humidity. Green line = amount of condensation on the window given by the right-hand axis..... 52

Tables

Table 1. Fit parameters of the power law pressure/flow model $Q=C(dP)^n$ 8

Table 2. Airtightness and ventilation configurations – year 1 (ventilating whole house, some ceiling ports opened). 17

Table 3. Airtightness and ventilation configurations – year 2 (ventilating Zone 2, ceiling ports closed). 17

Table 4. Symbols used in the nodal model equations..... 21

Table 5. General materials properties used in the nodal model simulations..... 23

Table 6. Mean, maximum and minimum infiltration rates at different airtightness levels for different regions around New Zealand. Values were deduced from the models shown above with units given in given in ACH @ atmospheric pressure..... 46

Table 7. Mean age of CO₂ and mean age of moisture..... 48

Table 8. Parameters output by WUFI Plus model of two Mosgiel-based homes using supply-only ventilation systems. 53

Table 9. Summary of results for DUD131 and DUD132. 55

1. Introduction

Ventilation and insulation, in conjunction with heating, are key components to keeping the indoor environment healthy and free of pollutant build-up. Ventilation in New Zealand is governed by New Zealand Building Code clause G4 *Ventilation*, where it is required that a building has openable windows equivalent to 5% of the buildings floor area. Balancing the required amount of additional ventilation with the background infiltration through adventitious cracks and gaps in the opening is a challenge when operating a dwelling.

The airtightness of a home is a key factor in estimating the level of background infiltration, which in turn provides information on the level of additional ventilation (if any) that may be needed. Earlier work at BRANZ (Bassett, 1986; 1985; 2001) compiled an airtightness database of 137 homes built from the 1930s to the mid-1990s. A summary of this is shown in Figure 1.

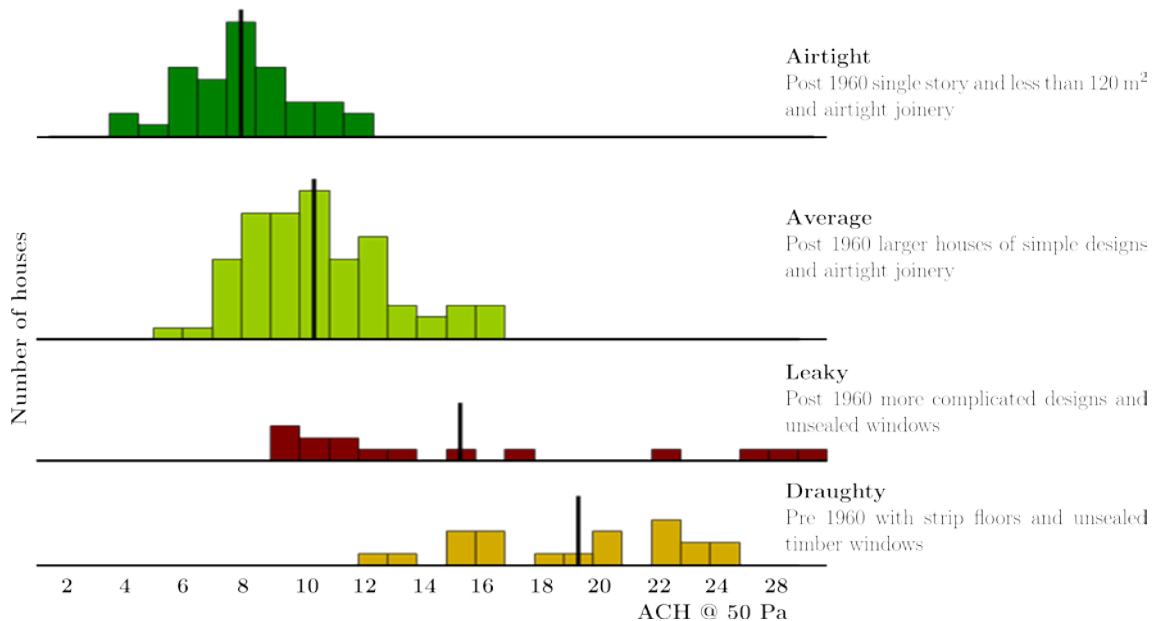


Figure 1. Summary of earlier airtightness in New Zealand.

This earlier work showed a clear trend to increased airtightness of New Zealand dwellings, independent of any changes to the Building Code. What was clear at the outset of the WAVE (Weathertightness, Air quality and Ventilation Engineering) programme was that there was a need to ascertain whether this trend was continuing and to determine the effect of this in light of G4, with the aim of helping to guide future changes to the Building Code.

The underlying assumption in G4 is that occupants will open their windows at regular intervals. However, anecdotal evidence suggested that this might not be the case, particularly during winter, and where occupants have security concerns or are away from the home during the day.

There is a significant anecdotal evidence that many households are unwilling or unable to operate windows regularly. With more airtight dwellings, it may become necessary to install mechanical ventilation. This could be of the form of a supply-only system that is common in the market now or a balanced system with heat recovery at the more

sophisticated end of the spectrum. Work in this report goes some way to clarifying the effectiveness of supply-only ventilation with regards to removal of moisture.

Earlier work on supply-only ventilation systems (Pollard and McNeil, 2010) has shown there is opportunity to improve control function performance both from the energy and moisture points of view. Work with the University of Otago Physics Department monitoring two homes in Mosgiel for 12 months has provided a dataset of in situ performance, which has been used as the basis of WUFI Plus models of the two homes. With these models, differing algorithms have been trialled to look at ways to improve the ability of supply-only ventilation to remove moisture but minimise the energy impact.

Onsite work at BRANZ has resulted in the development of an experimental facility where the airtightness (an intrinsic function of the building) can be easily varied. This facility allowed for the measurement of moisture removal performance of supply-only ventilation systems with respect to dwelling airtightness. Estimation of climatic effects on ventilation and infiltration were also completed.

Standard tracer gas techniques were used to measure air change rates for different ventilation options, and equipment was developed to monitor duct flows in situ.

1.1 Airtightness background

A value of airtightness for a building is commonly given as the number of building air changes per hour (ACH) at a pressure difference of 50 Pa across the building envelope. This unit is often denoted as ACH N_{50} or ACH @ 50 Pa.

The airtightness of New Zealand homes has increased over time, even though there is no requirement for airtightness in the Building Code (McNeil et al., 2012). The average N_{50} result from houses built before WWII was around 19 ACH, but this reduced dramatically to 8.5 ACH for houses built between 1960 and 1980. A significant contributor to envelope airtightening around 1960 was the shift from suspended tongue and groove flooring to sheet floor construction and slab-on-ground floors. Another change at a similar time was the shift from timber joinery to aluminium-framed doors and windows as well as a reduction of open fireplaces. This brought the opportunity to fit better air seals around opening windows and doors, at the same time improving the weathertight performance of domestic joinery. By the mid 1990s, the mean airtightness result was 6.7 ACH.

In the USA, Sherman and Chan (2003) reported a similar two-fold reduction in average N_{50} measurements over a similar time period. In this case, the changes were largely voluntary but were also influenced by the 'weatherisation programme' to improve the energy efficiency of low-income homes. In contrast, Stephen (1998) reports little change in the N_{50} measurements in UK houses over a similar period. Much more dramatic changes in N_{50} are reported in Canada and Sweden where mandatory airtightness targets were adopted to reduce the energy loss consequences of uncontrolled ventilation. A second driver of airtight construction in these cold climates is the need to control exfiltration to prevent interstitial condensation, which is less of a concern in more temperate climates.

Materials and construction practices have continued to influence the airtightness of houses. Recent examples of changes are the widespread use of bonded plaster cornice or a square-stopped interior plaster finish and the adoption of air seals around window and door assemblies. The latter is due to the adoption of Building Code Acceptable Solution E2/AS1 (Department of Building and Housing, 2005a), where it is required

that air seals are to be fitted around door and window assemblies. The aim was to improve the degree of pressure moderation across the joints between window frame and cladding and improve the weathertightness of what was seen as a weak point in window installation.

The first major component to the WAVE ventilation research programme was the performing of an airtightness and ventilation survey of newer housing stock to update the database. This survey provided airtightness data for newer (post-1994) houses and confirmed a continuing trend, which had a mean of 6.5 ACH for newer housing stock.

Airtightness can be taken as a proxy measure of mean infiltration rate. One can estimate this by simply dividing the N_{50} result by 20 to obtain a mean rate for the year, as the mean indoor outdoor pressure difference is around a 20th of the pressure during a blower door test. It must be stressed at this point that the /20 rule only gives a mean. Windier periods of the year will have infiltration above this result, and during calmer periods, the infiltration will be below this result. This approximate measure is also strongly influenced by local topography and exposure of the dwelling.

1.2 Ventilation and airtightness

In terms of ventilation, Building Code requirements for residential buildings are often quite unsophisticated in countries with temperate climates. New Zealand is no different. Occupants are expected to open windows for ventilation, and the Building Code offers Acceptable Solution G4/AS1 (Department of Building and Housing, 2005b) requiring window and door openings to be at least 5% of the floor area. It is clear from the airtightness measurements of older houses that window opening may have been unnecessary to meet ventilation needs because of the background infiltration. In newer houses, the changes in construction discussed above have closed down natural ventilation paths, and it may be necessary to actually open the windows for some time every day to provide adequate fresh air and dilute moisture and other indoor pollutants.

Given the straightforward method for estimating mean infiltration from the airtightness database, we compared the amount of ventilation provided in different New Zealand dwellings 'in use'.

In the past, it has been difficult to measure ventilation rates in homes because conventional tracer methods were too intrusive and expensive to use in large numbers of houses. This study used passive samplers and emitters that are more easily deployed (Dietz and Cote, 1982; Upton and Kukadia, 2011) to provide the first survey of ventilation achieved in New Zealand homes. In tandem with the airtightness survey, a study was made of mean ventilation rates over a 3–4 week period in the same sample. Results are presented below in Figure 2.

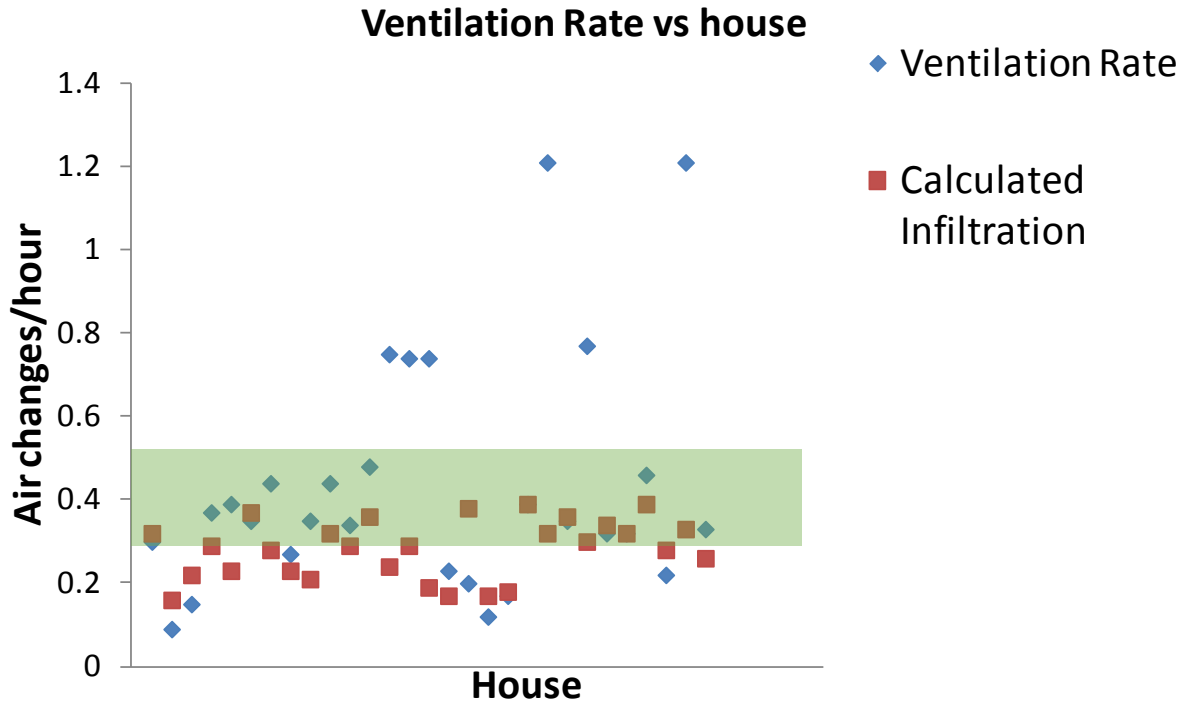


Figure 2. Estimated infiltration and measured ventilation. The green band indicates the range of acceptable ventilation rates in countries where there is a minimum rate defined. Note that flow rates are given as air changes per hour at atmospheric pressure.

Overlaid on the data is a band representing the range of acceptable ventilation rates in countries where there is a minimum rate set. What is clear from the measured ventilation rates is that about a third of the sample were underventilated relative to these standards.

In recent years, it has become common for occupants to add additional supply-only ventilation to control moisture. Houses with operational supply-only ventilation systems in the survey above generally had more than enough ventilation, but there were several cases where the ventilation system had been turned off.

The results above present opportunities in

- additional ventilation where occupants are not opening their windows
- tuning existing mechanical systems more effectively.

Ventilation has a large part to play in the control of indoor moisture. Indoor moisture has always been the most pressing indoor air quality issue in New Zealand houses. A 1971 survey (Trethowen, 1972) reported moisture problems in half of the surveyed houses, and later surveys (Buckett et al., 2011; Clark et al., 2005) have shown that little has changed.

Reference to ventilation in the current Building Code is made in clause G4, which specifies the area of openable windows a dwelling must have. However, when this requirement was made, New Zealand houses were built with a relatively high rate of infiltration. Opening windows supplemented the natural ventilation, but even with the windows closed, infiltration alone was typically enough to cope with most moisture loads.

Modern houses have been shown to be more airtight, leading to lower rates of infiltration that are not able to cope with the same moisture loads that were envisaged when clause G4 was originally written. Supplementing infiltration by opening windows depends entirely on occupant behaviour, and in some cases, this is not a practical solution.

This report provides an overview of the current housing stock and how New Zealanders currently ventilate their houses. This information is used later in this document to investigate the moisture removal effectiveness of supply-only ventilation systems relative to infiltration alone.

2. Equipment

2.1 The experimental building

The building shown in Figure 3. was constructed as a prebuilt shell in 2007 and transported onto the research site. The single-storey house has a floor area of 91 m² and a volume of 206 m³. The volume of the roof cavity is approximately 45 m³. The house is a traditional timber-frame construction that is clad with painted fibre-cement weatherboard directly fixed over a flexible wall underlay. The gable roof has corrugated mild steel cladding on timber trusses. The floor is made of particleboard, which is sealed with polyurethane. The walls and the ceiling are insulated to the requirements of the Building Code with fibreglass. All inner wall surfaces and the ceiling are lined with gypsum-based plasterboard, which received three coats of an acrylic paint.

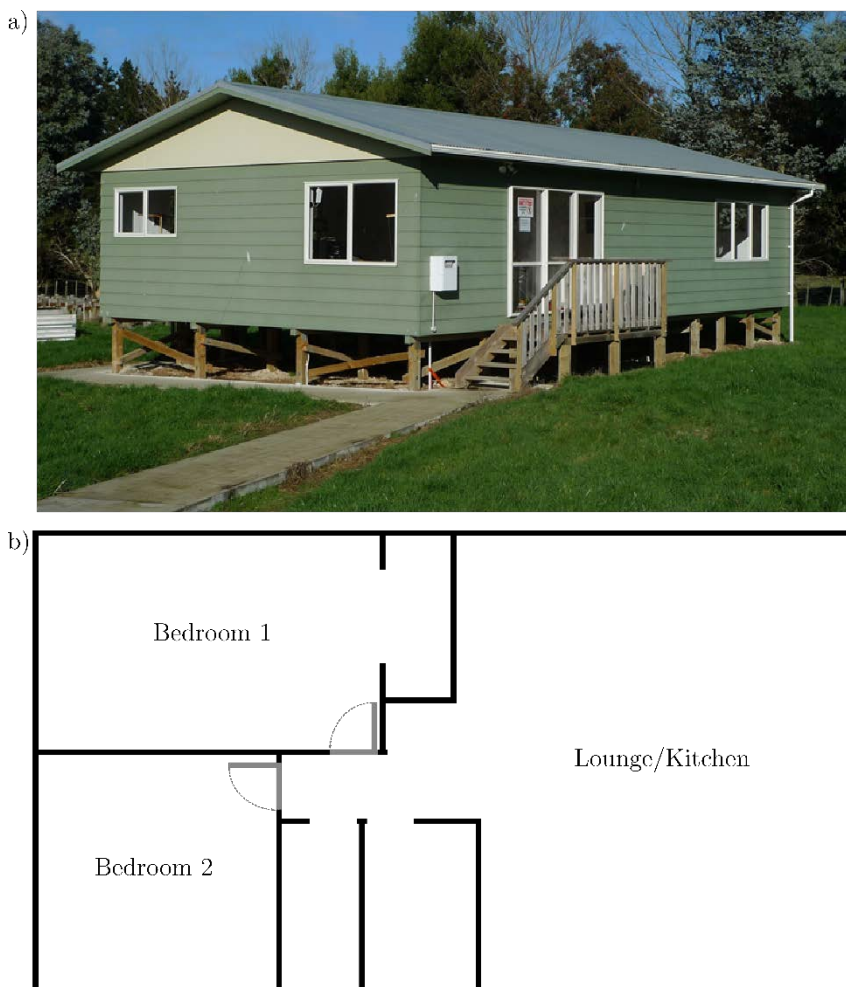


Figure 3. a) Photograph of the experimental building on site. b) Basic floor plan of the test building.

In order to study ventilation effectiveness at airtightness levels that are present in a large part of the New Zealand housing stock, we fitted the house with sealable ports that penetrate the envelope. The ports are located in the floor, walls and ceiling connecting the living area to the subfloor, cavity of the outer walls and attic respectively. Our intention was to reach an airtightness level as low as 1 ACH @ 50 Pa (all ports sealed) and an upper level of about 9 ACH @ 50 Pa (all ports open).

The prefabrication and the fact that it was going to be transported to its location on the research site made it necessary to achieve the airtightness through detailing of the indoor wall linings. Which were installed after the building reached its destination. We decided to implement the Canadian 'airtight drywall' approach. To avoid air leakage from the outer walls through the inner walls into the room, we isolated the inner wall by means of applying a 3 mm thick, closed-foam tape to the corners where the inner walls join onto the outer walls of the building. For the electrical outlets, we used flush boxes that have seals at the cable inlet and where the plasterboard butts on the box rim. To avoid air leakage through gaps between the floor and the ceiling boards, plasterboards were sealed using silicone caulking. All penetrations of the plasterboard for cables, lighting, access hatch to the attic and the like were sealed as best as possible.

2.1.1 Characteristics of the ports

In order to derive a model of the infiltration, we measured the pressure/flow characteristics of the ports by pressurising the building. The ports were constructed from PVC tubing with inner diameters of 38 mm and 64 mm. The ports were installed in the walls, floor and ceiling, which has given rise to four different pressure/flow characteristics.

These characteristics were determined by fitting an exponential function $Q = C(dP)^n$ to the measured data points. Figure 4 shows the measured data and graph of the fitted model, while the fit parameters are provided in Table 1.

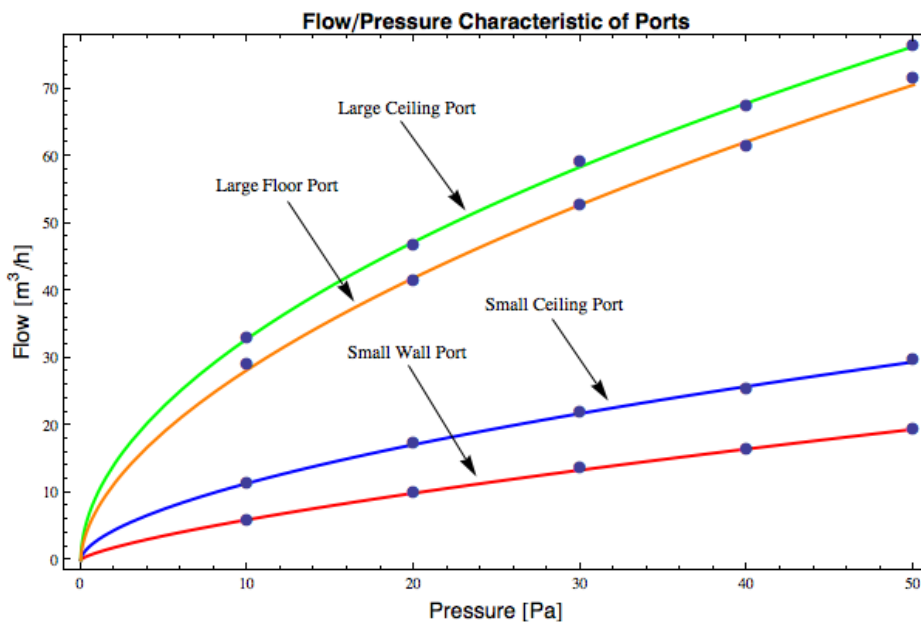


Figure 4. Measured data and fitted function for the flow characteristic of the various ports.

The diameter of the port is the dominant factor determining the flow/pressure characteristics. The flow characteristic of the small ceiling ports and the wall ports show comparatively little differences, taking into account that those ports lead on one hand into the large attic while the wall ports lead into the confined space of the wall cavity. This indicates that the outer shell of the walls is not very airtight and that the airtightness level of 1 ACH @ 50 Pa achieved in the house is largely determined by the inner wall lining.

Table 1. Fit parameters of the power law pressure/flow model $Q=C(dP)^n$.

Port location/Size	Coefficient C	Exponent n
Wall ports	1.1 ± 0.1	0.73 ± 0.02
Floor ports	7.6 ± 0.5	0.56 ± 0.02
Small ceiling ports	2.9 ± 0.1	0.58 ± 0.01
Large ceiling ports	9.8 ± 0.4	0.52 ± 0.01

2.1.2 Instrumentation

The building is equipped with instruments that allow it to run infiltration and contaminant removal measurements in a semi-automatic way. All operations are controlled by in-house BRANZ software, allowing a computer to control the indoor climate, sampling of the tracer gas and reading of temperature and humidity sensors. Measurement data is then written to a database (see Figure 5). A database table is used to describe indoor climate parameters such as temperature and humidity. The house can be heated and the humidity can be increased but no cooling or dehumidifying is available, apart from what the installed ventilation system is providing. Airflow through the ventilation system into each zone is measured by means of pressure-averaging tubes installed in the ducting.

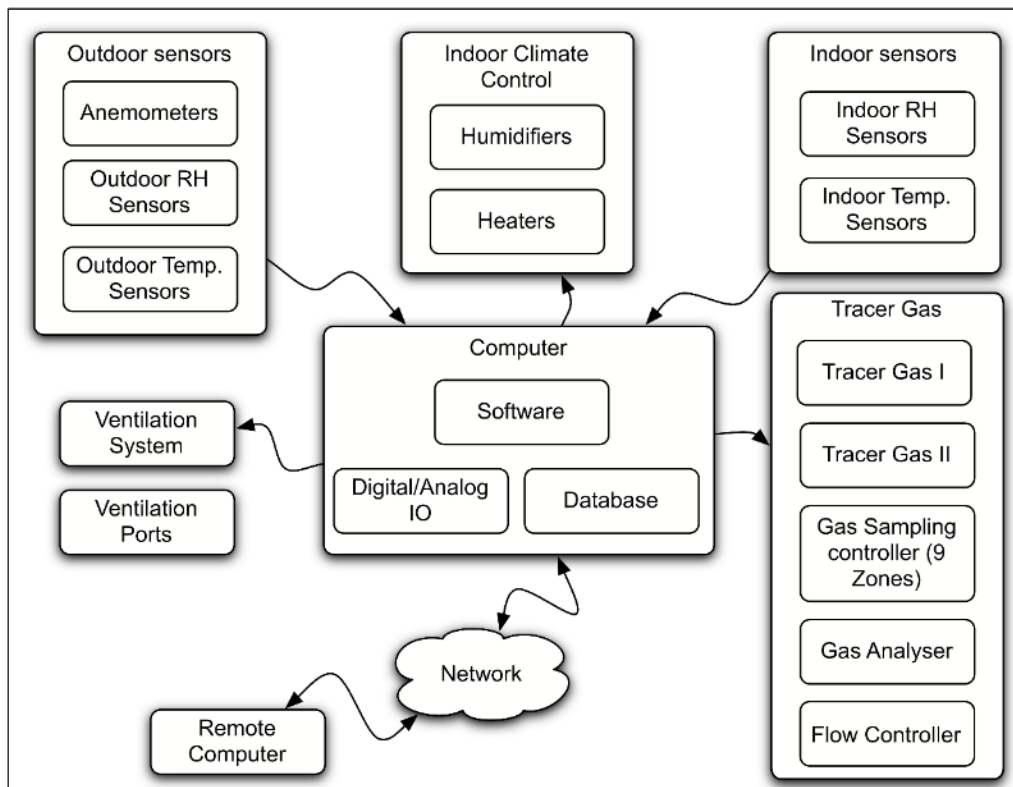


Figure 5. Instrumentation scheme used in the house.

The injection rate of each tracer gas is controlled by a Red-y Smart controller gas flow meter set via the computer. Flow rates can be adjusted between 0.8–40 mln/min for N₂ and between 1–140 mln/min for carbon dioxide (CO₂). An Innova 1412 photo acoustic gas monitor is equipped with filters to detect CO₂, Freon and sulphur hexafluoride (SF₆) with detection limits of 3.4 ppm, 0.02 ppm and 0.006 ppm respectively. The dynamic range of the gas monitor is typically 4–5 orders of magnitude.

The target working concentrations of the tracer gas in the zones is usually at least 10 times the detection limit or, in the case of CO₂, 10 times the background concentration. Tracer gases are sampled from the zones by means of a computer-controlled manifold that can switch each of the possible nine sampling locations onto the gas monitor.

Each room, including the attic, is equipped with a number of sampling and dosing tubes. In the living area, these tubes are located approximately 1.5 m off the ground. Before the gas monitor analyses the air sample, it purges the tubes and the sampling chamber to avoid cross-contamination. Measuring each location in turn takes about 10 minutes to process, thus allowing six samples to be taken from each location per hour. Outside temperature and wind velocities are obtained from a weather station located next to the house.

2.1.2.1 Pressure-averaging tubes

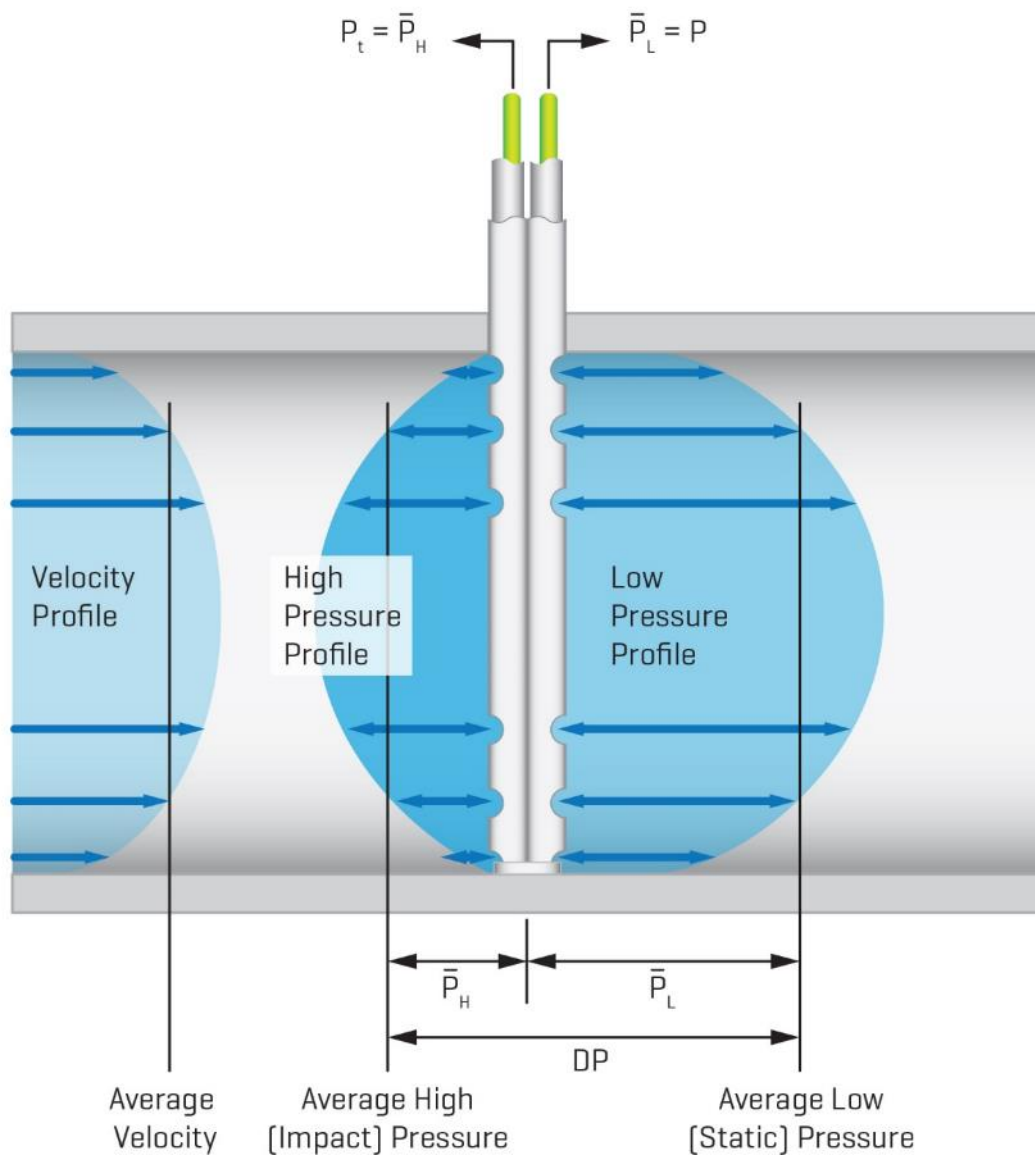


Figure 6. Pressure-averaging tube schematic. P_H and P_L represent the average impact and static pressures respectively. Adding them gives DP , which can be correlated to flow in the tube.

Pressure-averaging tubes were constructed in the lab to enable measurement of flow rates through ventilation ducts with a simple pressure transducer. This involved building an averaging pitot tube (see Figure 6) and installing it into a section of rigid ducting the same diameter as the ductwork under test. Constructed tubes were calibrated using a variable-speed fan and a laminar flow element, which produced a curve of output pressure versus flow.

2.2 Blower door – whole-house pressurisation

The blower door allows measurements of air leakage through the building envelope to be made via depressurisation of the building. This is achieved by measuring the flow through a calibrated orifice while a fan maintains a constant pressure across the envelope. Flow rates are measured for a range of pressures across the envelope before a curve fit to the data points is used to obtain a measurement of airtightness. A detailed description of the blower door technique can be found in Jensen (1986). It is from blower door measurements that an airtightness value in units of ACH @ 50 Pa are obtained.

3. Experimental methods

3.1 Airtightness and ventilation survey

3.1.1 Selection of houses

The airtightness and ventilation survey was split across four different cities in New Zealand – Wellington, Palmerston North, Dunedin and Auckland. A database of building consents was used to obtain a random sample of consents for houses built after 1994. A total of 36 homeowners agreed to take part in the survey. Of these 36 houses, eight had supply-only positive-pressure ventilation systems installed in the roofspace. All these systems distributed filtered roofspace air throughout the home depending on temperature measurements in the living space and roofspace.

3.1.2 Airtightness measurement

A blower door test to EN 13829 (2001) standard was completed on each of the 36 houses, and then the opportunity was taken to measure the contribution of a range of different leakage paths. This was carried out by progressively sealing up openings in the envelope and repeating the blower door test.

In general, the following three tests were completed on each dwelling:

- A standard N_{50} test with no openings sealed.
- A test with specific ventilation openings sealed. In most cases, these ventilation openings consisted of extract fans in bathrooms and kitchens, some of which were simply ducted to the roofspace (not outside).
- A final test with all obvious leakage openings sealed. The most obvious leakage openings to be sealed were around internal garage doors and defective seals around attic access hatches.

The airtightness measurements were also used to give an estimate of the mean infiltration through the envelope using the /20 rule of thumb described earlier:

$$\text{Estimated infiltration rate} \approx \frac{N_{50} \text{ result}}{20} \quad (1)$$

3.1.3 Mean ventilation rate measurement

Ventilation measurements were performed in 31 of the 36 houses during winter. Winter was chosen because it was perceived that ventilation would be at its lowest, i.e. windows open less often.

A perfluorocarbon tracer (PFT) technique (Upton and Kukadia, 2011) was used, with equipment and analysis supplied by the UK's Building Research Establishment (BRE). The technique involves deploying passive tracer gas sources and activated carbon sampling tubes in a building for a period of time. The resultant concentration of tracer in the sampling tubes can then be used to calculate an average ventilation rate.

Plans for each house were obtained to allow the room volumes to be precalculated. Key dimensions were measured upon arrival to ensure the plans matched the building, and any differences were marked on the plans and the locations of sources and samplers modified accordingly. The tracer sources were distributed around the home in a volume-weighted manner, with the bathroom being chosen as a reference volume in all cases. Figure 7. shows a typical floor plan.

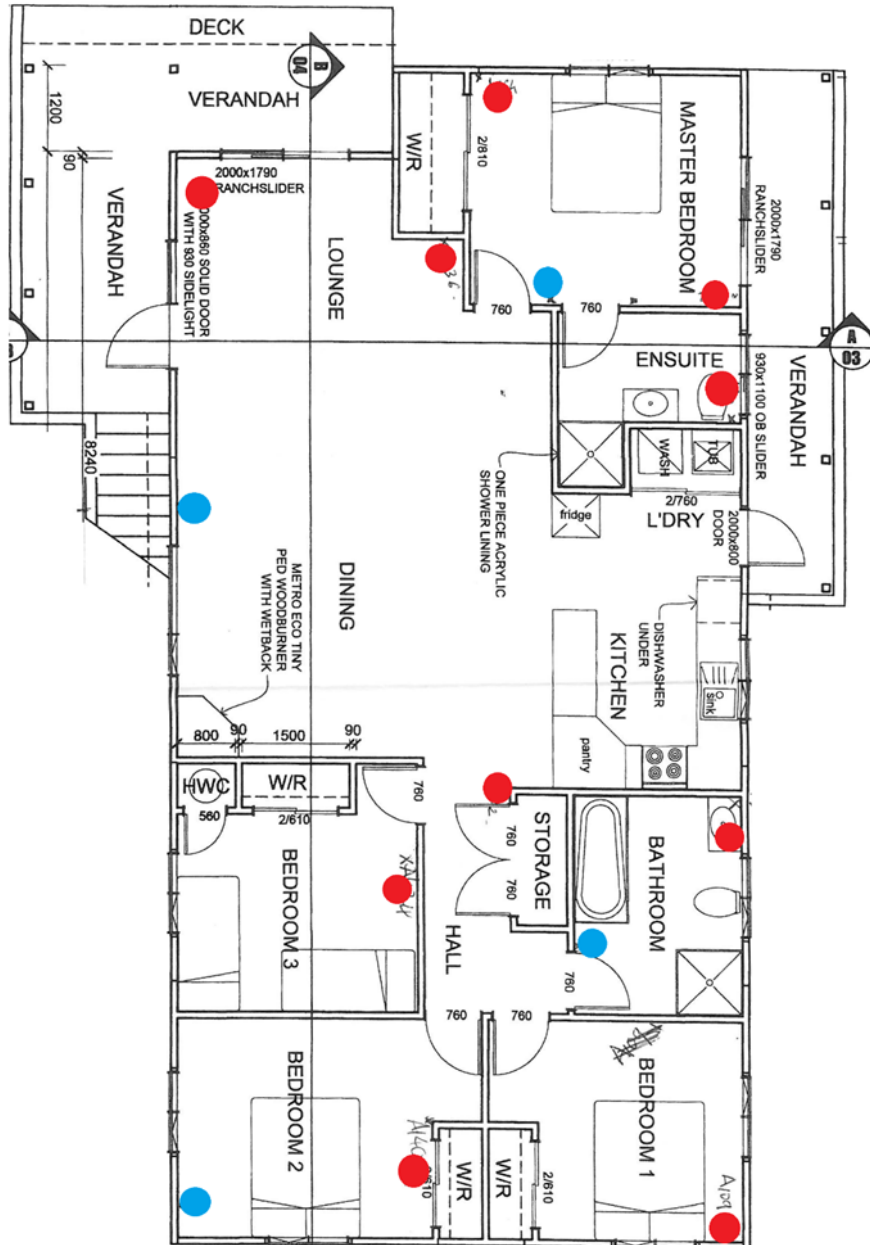


Figure 7. Typical distribution of tracer sources and sampling tubes (sources in red, samplers in blue).

Sampling tubes were placed in four rooms in each house, typically the lounge, bathroom, kitchen and master bedroom. These were left in place for at least 3 weeks, but sometimes this was as long as 4 weeks because of occupants' unavailability to schedule removal.

There were several important considerations when it came to the location of the source and sampling tubes:

- Source and sampling tubes need a good degree of separation to ensure the sampler collects tracer that has been well mixed in the zone.
- Both sources and sampling tubes need to be located as far as practicable from windows/doors to allow incoming air to mix within the zone.
- Temperature has a direct influence on the emission rate. The sources should not be in direct sunlight or within 1.5 metres of heat sources. The temperature was also measured at each source location using Dallas DS1923 iButtons.

3.2 Experimental building

3.2.1 Tracer techniques

Tracer gas measurement techniques are a well established means of measuring air change rates in enclosed spaces. They generally involve releasing a tracer gas (by one of several methods) into a space at a concentration significantly above background and measuring the resultant concentration in the space over time. The limitations of the different measurement techniques are well known (Liddament et al., 1983; Liddament, 1986) and are covered briefly here.

The standard techniques are step up, step down, constant concentration and constant emission.

Both the step up and step down tracer techniques produce an estimate of air change over a short period of time. The constant concentration technique is difficult to achieve in a multizone experimental environment. Time constants of measurement equipment and the changing of sampling zones make it problematic to achieve fast enough measurement response to control the tracer dosing accurately.

Therefore, as the WAVE programme required a measurement of continuous ventilation rate, the constant emission technique was chosen. Simply put, the emission rate of the tracer is kept constant, and the concentration in the different measurement zone(s) recorded. From here, the air exchange rate can be calculated.

A typical experiment involved adding a 'preflood' dose of tracer gas to the space of interest, then lowering the tracer dose rate to a much smaller constant value. This avoided lengthy waiting periods for the tracer concentration in the zone to come to an equilibrium. This technique scaled well from single-zone to two-zone or even three-zone experiments.

Three tracer gases were available for the work in this report – SF₆, CO₂ and Freon 134a.

Measured concentrations from the gas analyser were used in the mass balance equation in the following section, with the aid of a matrix solver to calculate the air exchange rates.

3.2.2 General mass balance equation

Ventilation rates were calculated using a standard mass balance equation (Rudd et al., 2009; Sherman, 1998):

$$V \frac{dC(t)}{dt} = Q[C_e - C(t)] + F \quad (2)$$

Where,

- V = enclosure volume [m³]
- Q = airflow through enclosure [m³/s]
- C_e = external tracer concentration [kg/m³]
- $C(t)$ = internal tracer concentration at time t [kg/m³]
- F = tracer dosing rate [kg/s]

The following data from the measurements was required to solve the system of equations:

- Concentrations of all tracer gases in their respective zone.
- Temperature of the air in each zone.
- Dosing rate of each tracer.

The results were then averaged to give interzonal flows on an hourly basis.

3.2.3 Distribution of sampling and dosing points

For all experiments (unless otherwise noted), tracer gas sampling locations were distributed around the zones of interest in a volume-weighted manner. In a two-zone experiment, Zone 1 typically had eight dosing and sampling locations, and Zone 2 had two. Samples were returned to the same zone they were sampled from via the manifolds at the gas analyser. Once the building was dosed with tracer gas, the differences between measured concentrations at different location in the same zone were negligible, suggesting the air in each zone was well mixed. This is investigated further in section 3.2.5.

3.2.4 Infiltration experiments – building characteristics

Measurement of infiltration rate – single zone

Before the performance of various ventilation systems was determined, the infiltration characteristics of the house at different airtightness levels in the absence of a ventilation system had to be established. As most experiments undertaken in the building were completed at one of the four airtightness levels of 1, 3, 5 and 9 ACH @ 50 Pa, infiltration was studied at these configurations. Various ports in the walls, the ceiling and the floor were opened to achieve these levels of airtightness. A ventilation port plan was used to make sure that only those ports were opened at a given airtightness level that allowed for an even distribution of air leakage paths throughout the building. After an initial flooding of tracer gas, the injection rate of the tracer gas was adjusted in accordance with the set airtightness level to reach a tracer gas concentration of at least 10 times the detection limit, thus allowing for enough dynamic range and lower signal-to-noise ratio.

Tracer gas concentrations for the building were recorded on a 10-minute basis and, together with the local climate (both temperature and humidity, indoors and out), recorded to the database.

3.2.5 Mixing experiments

Tracer gas concentration can only be sampled at discrete locations within a zone, leading to the assumption that the tracer gas is homogeneously mixed with both the air already present in the zone and the air that is entering the zone (Sherman et al., 2014). However, it has been shown that tracer gases do not always perfectly mix within a zone such that infiltration rate measurements can be influenced by tracer gas sampling positions (Barber et al., 1984; Lunden et al., 2012; Maldonado et al., 1983; Van Buggenhout et al., 2009).

A common solution to incomplete tracer gas mixing is to incorporate a fan into the set-up to artificially mix the air and ensure concentration homogeneity of the tracer gas (Chao, 1994; Lunden et al., 2012). However, mixing the air by means of a device such as a fan can introduce errors in the infiltration measurement if the device is driving ventilation, as reported by Shao et al. (1994).

The horizontal and vertical mixing of a tracer gas released inside a test building without the use of an artificial mixing device was examined. The influence of solar radiation on the mixing process was investigated, and an estimated error associated with incomplete mixing for this scenario was obtained.

Experimental procedure

Figure 8 shows part the floor plan of the unoccupied test house described in section 2.1 Only two rooms of the test house were used during this experiment – the northern (sun-facing) zone, labelled Zone 1, and the south-facing zone, labelled Zone 2. Separate experiments were conducted in the two zones to determine the tracer gas mixing for different vertical heights and for different horizontal positions across each zone. The zone door was kept closed during experimentation. No artificial mixing devices were used, and the test building was unoccupied while the experiment was running.

To prevent cross-contamination of tracer gas between zones, experiments conducted in the two zones illustrated in Figure 8 were carried out at different times. Similarly, horizontal and vertical mixing experiments were also conducted separately.

The constant emission technique described in section 3.2.1 was used to determine the infiltration at different vertical and horizontal points in each zone. For vertical mixing tests, sampling tubes measured SF₆ concentration at the centre of the zone at three different heights – 55 mm, 1065 mm and 2065 mm from the floor. Figure 8 illustrates the locations of the sampling points for the horizontal mixing tests. Each sampling point in the horizontal tests was 1600 mm above the floor of the zone.

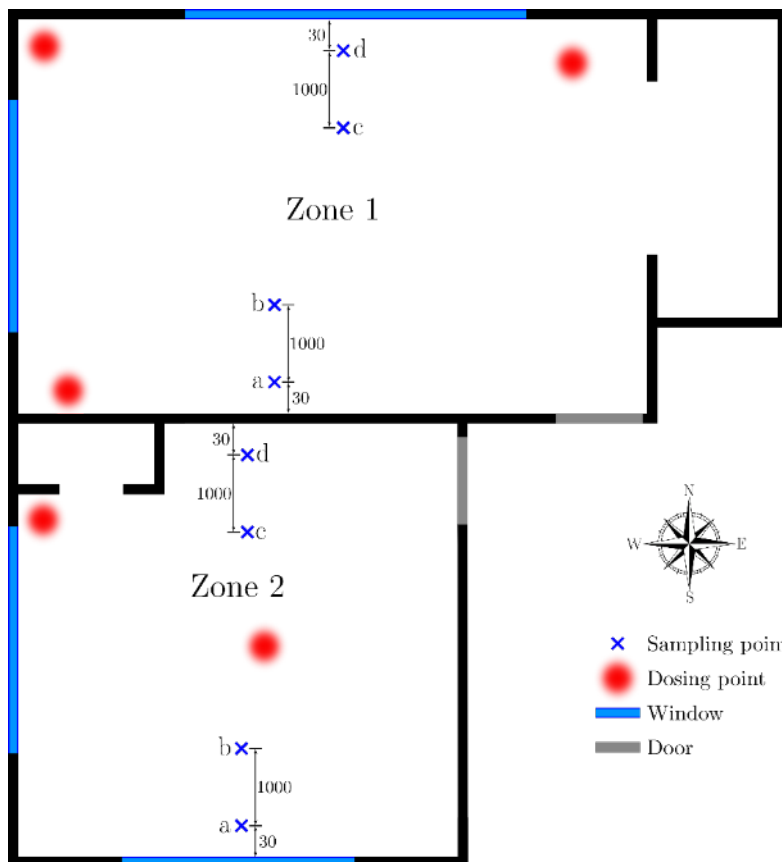


Figure 8. Locations of the sampling and dosing points in Zones 1 and 2 for horizontal mixing experiments. All sampling points were at a height of 1600 mm from the floor. Distances indicated in the figure are in units of mm.

3.2.6 Ventilation and infiltration experiments – two zone

Ventilation measurements were undertaken during experiments looking at the effectiveness of ventilation systems with respect to removal of moisture (see section 3.2.8). These experiments were carried out during the autumn-spring period over consecutive years. These were two-zone measurements treating Zone 2 as a separate zone with the door closed (see Figure 9. and Figure 10.).

To measure ventilation rates, two tracer gases were used. These were dosed into the main part of the house and bedroom space in accordance with the constant emission method (see section 3.2.1). The experiments took place in late autumn and early winter. Both tracer gases were introduced at an accelerated rate to get to an estimated equilibrium concentration, and the dosing rates were dropped to an adequate rate for the expected air exchange rate before experiments began. Concentrations of all gases in each zone were obtained every 10 minutes from the gas analyser.

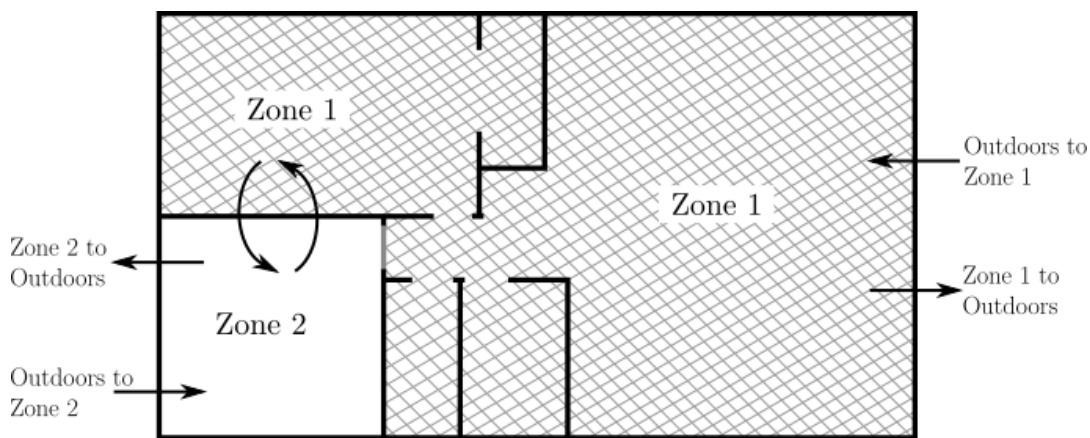


Figure 9. Building floor plan showing Zone 2 as the smaller bedroom.

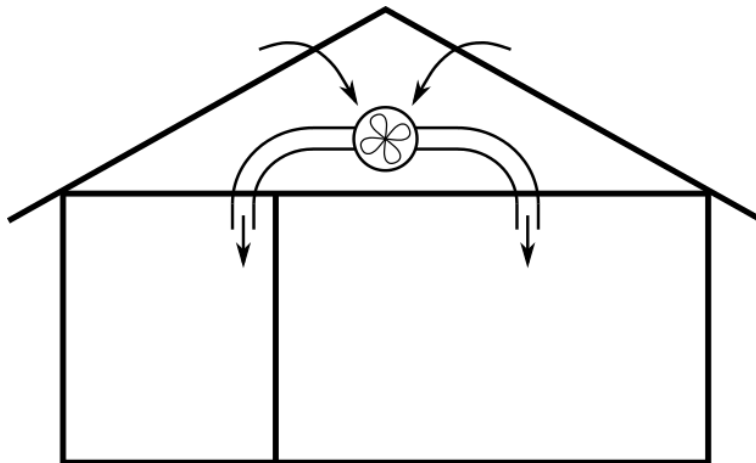


Figure 10. Two-zone ventilation – supply-only roofspace system.

During year 1, the house was run over the following four airtightness levels – 1, 3, 5 and 9 ACH @ 50 Pa. It was also run with and without a supply-only ventilation system at each of the configurations. The ventilation system was ventilating both Zone 1 and Zone 2 in these experiments. Also during year 1, the default control regime for the ventilation systems was active, controlling ventilation on the temperature of the dwelling and roofspace. In year 1, ceiling ports were also opened for some airtightness levels, which led to some recirculation of ventilation air. Year 1 configurations are summarised in Table 2.

Table 2. Airtightness and ventilation configurations – year 1 (ventilating whole house, some ceiling ports opened).

Ventilation (whole house)	Airtightness (ACH @ 50 pa)				
	1	3	5	6.5	9
Supply only	x	x	x		x
Infiltration only	x	x	x		x

In year 2, the configuration was changed to limit the airtightness setting to 1, 3, 5 and 6.5 ACH @ 50 Pa. This was necessary to remove the impact of the recirculation effect by opening ceiling ports. As the ceiling ports contributed a significant amount of the leakage available in the building, the uppermost airtightness configuration was limited to 6.5 ACH @ 50 Pa.

During year 2, the ventilation system was also altered to supply air to Zone 2 only, and this time, the system was altered to ventilate at a constant rate to remove the effect of the control regime. See Table 3 for a summary of the experimental configurations during year 2.

Table 3. Airtightness and ventilation configurations – year 2 (ventilating Zone 2, ceiling ports closed).

Ventilation (one room only)	Airtightness (ACH @ 50 pa)				
	1	3	5	6.5	9
Supply only	x	x	x	x	
Infiltration only	x	x	x	x	

3.2.7 Moisture removal effectiveness

Dosing two zones with moisture

With the building configured for two zones as per section 3.2.6, moisture was introduced into Zone 2 using a humidifier (McNeil et al., 2014). A dosing rate similar to two sleeping adults (Plathner, 2001) was chosen, as it represented a reasonable in-use moisture load.

As the humidifier output (approximately 1 kg/hr) was more than two sleeping adults would generate, it was pulsed on for 1 minute intervals every 5 minutes to give an effective moisture introduction of 0.16 kg/hr over the dosing period, for a total of 1.28 kg.

Each dosing period ran for a total of 8 hours, beginning at 10pm and finishing at 6am. This experimental pattern was completed for both experimental years for the configurations shown in Table 2 and Table 3.

In year 2, the configuration was changed to limit the airtightness setting to 1, 3, 5 and 6.5 ACH @ 50 Pa. This was necessary to remove the impact of the recirculation effect by opening ceiling ports. As the ceiling ports contributed a significant amount of the leakage available in the building, the uppermost airtightness configuration was limited to 6.5 ACH @ 50 Pa.

During year 2, the ventilation system was also altered to supply air to Zone 2 only, and this time, the system was altered to ventilate at a constant rate to remove the effect of

the control regime. See Table 3 for a summary of the experimental configurations during year 2.

Mean age of air and moisture

Local mean age calculations were made of both the CO₂ dosed into Zone 2 and the introduced moisture. Mean age calculations can be difficult when there are no exhaust vents. Publications (Sandberg, 1983; Haghghat et al., 1990; Bassett, 2000; Nordtest Method, NT VVS 118; Nordtest Method, NT VVS 019) detail techniques for achieving this and define the relative contaminant removal effectiveness.

The mean ages (τ_p) of CO₂ and moisture were calculated using (Nordtest Method, NT VVS 118):

$$\tau_p = \frac{C_p}{(F/V)} \quad (3)$$

Where,

C_p = steady state tracer/water concentration

F = tracer/water emission rate

V = volume of the room

The mean age of CO₂ and moisture were calculated from the above-mentioned set of dosing experiments. The resulting changes in humidity were observed and the data from the temperature and humidity probes used to calculate the density of water vapour in the zone air.

3.2.7.1 Modelling

Rode model

An analytical model was used to simulate the dosing experiments, with the aim to allow extrapolation of measurements to other climate zones in New Zealand. The model required hourly averaged ventilation data and the amount of introduced moisture. Results were then compared to the calculated values based on the vapour density of air in the room.

The air and walls of Zone 2 were modelled taking the same approach as that developed by Rode et al. (2001). The transport equations are based on the humidity ratio of the air. The basic form of the model is given by:

$$V \cdot \rho_{air} \frac{x^{new} - x^{old}}{\Delta t} = \sum G \quad (4)$$

Where,

V = the volume of the room [m³]

ρ = air density [kg/m³]

x = humidity ratio of the air [kg/kg]

G = a source term [kg/s]

The source term was summed over the various sources available – different source terms can be written for different source types (see Equations (5) and (6).)

The source term for ventilation air is:

$$G = n_{vent} V \rho (x_{vent} - x_{air}) \quad (5)$$

Where,

n_{vent} = the number of airchanges per unit time [h^{-1}]

x_{vent} = the humidity ratio of the source air [kg/kg]

x_{air} = the humidity ratio of the air in the zone [kg/kg]

The source term for emission from an absorptive surface is:

$$G = A_{surf} \beta (p_{surf} - p_{air}) \quad (6)$$

Where,

A_{surf} = the available surface area in the room [m^2]

β = the surface transfer coefficient of the surface [$\text{kg}/(\text{m}^2\text{sPa})$]

p_{surf}, p_{air} = the partial pressures of water vapour on the surface and room air respectively [Pa]

Once the sum of the sources was found using Equations (5) and (6), the new humidity ratio was calculated by rearranging Equation (4). The moisture dosing experiments were carried out simultaneously with the ventilation measurement (see section 3.2.6) so that hourly mean ventilation rates were available to the model.

Humidity ratios were first calculated for each sensor location, and the ventilation rates used were taken from the hourly datasets (see section 3.2.6). The surface area of Zone 2 was taken as 47 m^2 , with a typical surface transfer coefficient of $2 \times 10^{-10} \text{ kg}/(\text{m}^2\text{sPa})$. Surface temperature and humidity were taken as the measured values inside the wall just behind the lining.

Nodal model

For year 2, a more sophisticated nodal model, developed by BRANZ, was used to model the humidity in the room.

In this context, a nodal model is an abstraction of building components and their physical properties and interaction onto a small number of points (nodes) and their connections (edges). It represents the bulk properties of building components or materials and their interaction with the surrounding.

Property changes within the material or component are usually not considered. For example, if the top of a cladding has a temperature of 20°C and the bottom has one of 18°C , a single node will show the bulk material temperature of 19°C .

This can only be overcome by introducing more nodes, in this example, a top node and a bottom node with a thermal resistance equal of that of the cladding material and its thickness. By adding more and more nodes, in principle, the model can be made arbitrarily complex representing more and more aspects of the physical system.

The nomenclatures of nodes and edges are taken from graph theory because of the resemblance of nodal models with graphs.

The schematic in Figure 11. shows an example of how nodes are allocated to building components that make up the physical system under investigation. In the case below, only one node is placed for each component. It is, however, also possible to place multiple nodes into one component in cases where a better special resolution is required.

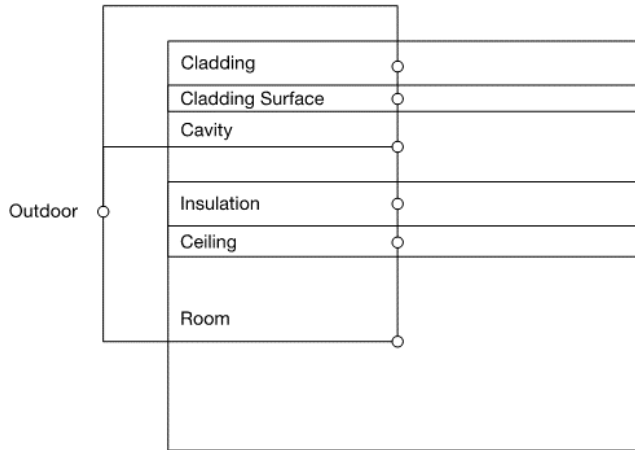


Figure 11. Nodes in building components describe the building as a physical system.

The nodal model as implemented for this research has the environment always in the first node, which then drives the temperature and humidities of the other nodes according to their transport resistances and so on. The implementation of the nodal model allows driving the temperature of other nodes by means of an interpolation function, which is used instead of the initial temperature value. This means, however, that this node's temperature will not be solved for. The humidity of the nodes cannot be set via an interpolation function in this implementation but needs to be solved for. In case the humidity for a node needs to be altered over time, a moisture source/sink needs to be declared for that node.

Figure 12 shows a small detail of a roof nodal model as represented within Mathematica. The points represent the nodes and are material properties while the lines (edges) represent the resistances or conductances between the nodes. The use of the nodal model is not restricted to the application in building physics. It can be applied to the solution of many dynamic systems in which the bulk properties of components and their interaction need to be modelled.

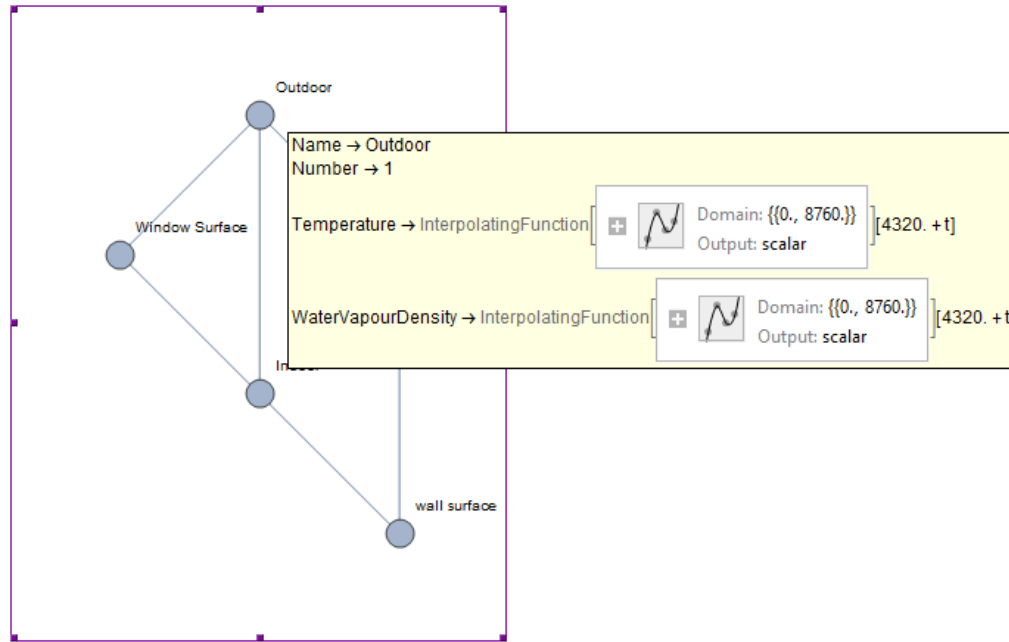


Figure 12. Section of the graphical representation of a nodal model with an edge property overlay.

As with any modelling and simulation, it is good practice to have a benchmark against which the performance of a model can be assessed. Benchmarking helps to avoid creating models that cannot replicate measurements conducted on real buildings or building components. It allows to fine-tune the model to reflect reality as close as possible given the resolution of the model.

Once the benchmarking has been done, model parameter changes, for example, changes in outdoor climate, can then simulate how the building would perform under conditions that are different to those at the time of the measurement.

Nodal model mathematics

In this section, the mathematical formulas used to describe the nodal model are presented and described.

The equations are describing a coupled system of first-order differential equations that need to be solved simultaneously. For each node, there is one mass and one heat equation describing the properties and flows of heat, air and moisture to and from that node.

The symbols used in the equations are described in Table 4..

Table 4. Symbols used in the nodal model equations.

Symbol	Unit	Comment
A_{ij}	m^2	Area between nodes i and j
c_i	$J/kg\ K$	Specific heat of material at node i
c_p	$J/m^3\ K$	Specific heat of air at constant pressure
F_{ij}	m^3/s	Air exchange rate from node i to node j
h_{vij}	W/m^2K	
L_{ij}	J/kg	Latent heat
m_i	kg/m^3	Vapour density
m_i'	kg/m^3	Vapour density at next time step

p_i	Pa	Water vapour pressure at node i
r_{ij}	Ns/kg	Water vapour transport resistance between nodes i and j
ρ_i	kg/m ³	Material density of node i
ϑ_i	kg/m ³	Concentration of condensate in node i
t	s	Time
T_i	K	Temperature at node i
U_{ij}		Thermal conductance between nodes i and j
V_i	m ³	Volume of node i

The model solves the mass equation (Equation (7)) for vapour density, that is, kilograms of water per cubic metre of material that is represented by the node.

The rate of change in vapour density at a node i is driven by the vapour pressure difference between node i and all other nodes in the system plus the net inflow of moist air from other nodes and the flow attributed to convection.

$$V_i \left(\frac{m'_i - m_i}{\Delta t} \right) = \sum_j \left(A_{ij} \frac{p'_j - p'_i}{r_{ij}} + V_i (F_{ji}^i m'_j - F_{ij}^i m'_i) + A_{ij} h_{v_{ij}} (p'_j - p'_i) \right) \quad (7)$$

The energy flow is governed by Equation (8), where the rate of change in temperature at node i depends on the temperature difference and the thermal conductance between node i and all other nodes, the infiltration and exfiltration of air and the latent heat of evaporating or condensation moisture.

$$\rho_i c_i V_i \left(\frac{T'_i - T_i}{\Delta t} \right) = \sum_j (A_{ij} U_{ij} (T'_j - T'_i) + c_p V_i (F_{ji}^i T'_j - F_{ij}^i T'_i)) + V_i L_{ij} \left(\frac{\Delta \vartheta_i}{\Delta t} \right) \quad (8)$$

The term $\frac{\Delta \vartheta_i}{\Delta t}$ in Equation (8) represents the amount of condensate/evaporate that has been accumulated during the time step Δt . This amount can be written as follows:

$$\frac{\Delta \vartheta_i}{\Delta t} = \frac{d(m - m_{sat})}{dt} \quad (9)$$

The saturation vapour density depends only on the temperature of the node so that the equation can be rewritten in a form that allows easier calculation:

$$\frac{d(m - m_{sat})}{dt} = \frac{dm}{dt} - \frac{dm_{sat}}{dT} \frac{dT}{dt} \quad (10)$$

With this, the energy equation can be rewritten to:

$$\frac{dT_i}{dt} = \frac{\sum_j (A_{ij} U_{ij} (T'_j - T'_i) + c_p V_i (F_{ji}^i T'_j - F_{ij}^i T'_i)) + V_i L_{ij} \frac{dm_i}{dt}}{\rho_i c_i V_i + V_i L_{ij} \frac{dm_{sat}}{dT}} \quad (11)$$

Each node contains the properties of the material that the node is going to represent in the simulation such as heat capacity, density, emissivity, volume and radiative area as well as the initial conditions of temperature and humidity.

Materials and resistances

Table 5 lists all materials and their properties used in the nodal models described later in this report.

Table 5. General materials properties used in the nodal model simulations.

Material	Vapour permeability [kg/m s Pa]	Thermal conductivity [W/m K]	Density [kg/m ³]	Heat capacity [J/kg K]
Air	2*10 ⁻¹⁰	0.0257	1.2	1005
Steel	10 ⁻²⁰	45	7860	420
Wood	-	0.1	500	2500
Gypsum board	4.2*10 ⁻¹¹	0.17	800	1090
Fibreglass	150.94*10 ⁻¹²	0.0473	16	848

3.2.8 CONTAM modelling

CONTAM is a multizone airflow and contaminant transport analysis software package designed by the National Institute of Standards and Technology (NIST) in the USA.

The software allows us to specify parameters for different airflow paths across the building envelope and calculate the infiltration rate due to all the airflow paths for user-defined internal temperatures and external temperature and wind velocities.

The dynamics of each airflow path in our CONTAM models were described using a powerlaw model that depends on the relationship between the flow Q and the pressure difference dP across the airflow path:

$$Q = C(dP)^n \quad (12)$$

The flow coefficient C and flow exponent n in Equation (12) are defined by the user in each simulation.

3.2.9 Two-zone ventilation and infiltration model

In order to extrapolate results of two-zone experiments to other areas of New Zealand, a two-zone CONTAM model was created of the experimental building. The two-zone model began with a base model for the most airtight case of 1 ACH @ 50 Pa. Subsequent models were created with extra flow paths added to account for the additional leakage openings as airtightness was reduced. The parameters for the additional flow paths were taken from blower door tests at the different airtightness levels.

Two variants of each model were created, both with and without a supply-only ventilator. An example floorplan of the CONTAM model for 1 ACH @ 50 Pa with supply-only ventilation included is presented below as Figure 13.

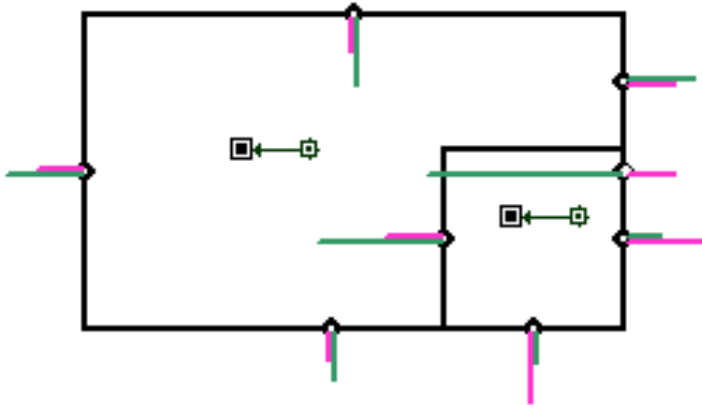


Figure 13. CONTAM two-zone model floor plan – 1 ACH @ 50Pa case shown.

Comparison was made between the calculated results of these models and measured results from the tracer gas experiments (see section 4.5.3).

3.3 Control system evaluation

Two homes in Mosgiel, Dunedin, labelled here as DUD 131 and DUD 132, were instrumented in mid-2013 with the aim to collect in situ temperature, humidity and flow data for the home and ventilation system. Instruments were removed in early 2015. Data was collected with the same in-house BRANZ measurement system as used in the experimental building.

Temperature and humidity were monitored in the following locations (see Figure 14.):

- Inside the home (the same room as the main ventilation duct).
- In the roofspace.
- Inside the ventilation system ductwork.
- Outside.

Temperature was measured using type T thermocouples, and humidity was measured with Honeywell HIH5000 humidity probes. Flow of the ventilation system was monitored via a pressure-averaging tube (see section 2.1.2.1) installed in line with the system fan. The pressure output of the pressure-averaging tube was measured using a GEMS differential pressure transducer (0–62 Pa range). Due to the power output of the fan in one of the homes, a second differential pressure transducer (0–120 Pa range) was added in parallel to the first, as the signal was found to be clipping after several months on monitoring.

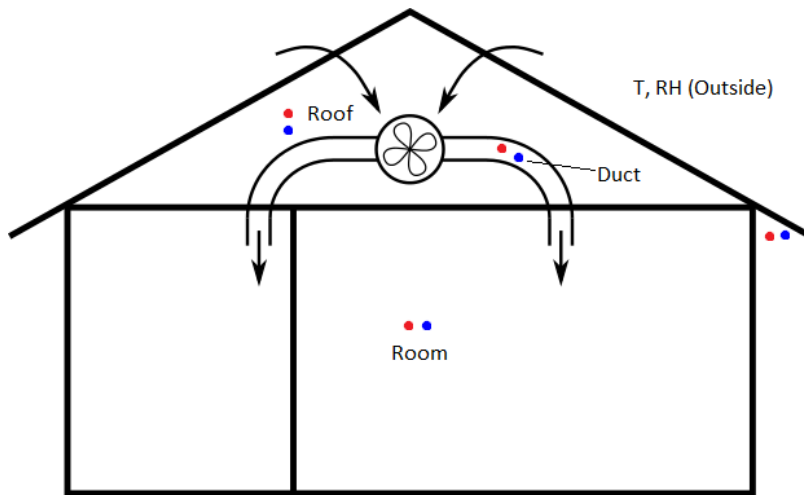


Figure 14. Sensor layout in Dunedin homes – red and blue dots indicate temperature and humidity sensors respectively.

3.3.1 WUFI Plus modelling

Models of both houses were constructed using WUFI Plus software (v.2.5.4.0). WUFI stands for 'Wärme Und Feuchte Instationär', which is German for 'transient heat and moisture'. WUFI software allows dynamic (time-varying) calculations of heat and moisture transport in multilayered building elements using coupled equations. The WUFI Plus version allows three-dimensional buildings to be constructed using a GUI interface. WUFI Plus has been developed by the Fraunhofer-Institut für Bauphysik (IBP, the Fraunhofer Institute for Building Physics), one of the 66 institutes and research units that make up Fraunhofer Gesellschaft. BRANZ has worked with IBP on improving WUFI Plus.

The aim of the modelling was to quantify the transfer of moisture and heat from the roofspace into the interior of the house due to the theoretical operation of the positive-pressure mechanical ventilation systems using different prototype control algorithms.

WUFI Plus models were created for each house using the closest equivalent match for materials in the WUFI database. The WUFI Plus models were set up and run with actual flow rates. Zone 2 'Interzone' was set to flow rates coming from Zone 1 based on output flow rates using the prototype control algorithms but with the monthly sets of hourly means put through the Matlab function `mssgolay` (Savitzky and Golay peaks-preserving smoothing algorithm adapted to allow non-uniformly spaced input data).

This smoothing was found to be necessary previously because WUFI Plus gave erroneous moisture results (underestimates by an order of magnitude) because the model solver is not good at resolving steep gradients that are present in the spikey data.

Prototype control algorithms

Four different prototype control algorithms were developed with different objectives in mind. In all four cases, the measured data (hourly averages of measured relative humidity (H), temperature (T) and derived absolute humidity (Q) in the roof and room) were used to calculate a flow rate for the positive-pressure mechanical ventilation system. The output is a flow rate ($L s^{-1}$). In each case, there is no feedback from the modelled temperature or humidity in the room through the control algorithm. In the future, it would be interesting to incorporate this feedback into the control algorithms.

Two algorithms given by Equations (13) and (14) have been developed with the intention of using the positive-pressure mechanical ventilation system to reduce the absolute humidity in the room while also increasing the temperature in the room.

The *BangBang_QDiff_And_TDdiff* algorithm (Equation (13)) is the most likely to achieve this goal, as the flow is only on if the absolute humidity is lower in the roof than in the room and the temperature is higher in the roof than in the room. Because the absolute humidity is not a function of temperature but just the water content of the air, this function is most likely to result in the biggest decrease in absolute humidity in the room. The output is scaled by $K = 50$ and 108 for DUD 131 and DUD 132 respectively so that the maximum flow rate is similar to the measured maximum flow rate for each house.

$$BangBang\ TDiff = K * (Q'_{roof} < Q'_{room}) \wedge (T'_{roof} > T'_{room}) \quad (13)$$

$$BangBang\ TDiff = K * (H'_{roof} < H'_{room}) \wedge (T'_{roof} > T'_{room}) \quad (14)$$

Most humidity sensors measure relative humidity rather than absolute humidity, so Equation (14) is provided as a possible alternative that might be easier to implement with affordable sensors without needing to calculate absolute humidity.

The existing control algorithm outputs a flow rate with a non-zero baseline level and a higher flow rate at other times. In order to directly compare the difference between operating with and without this continuous baseline flow, an algorithm similar to Equation (14) but with a constant base flow rate was tested – Equation (15). In Equation (15), the low baseline is represented by $C_{base} = 40$ and 20 for DUD 131 and DUD 132 respectively and $K_{base} = 10$ and 88 for DUD 131 and DUD 132 respectively when the relative humidity in the roof is less than that in the room and the temperature in the roof is greater than that in the room.

$$BangBang\ TDiff = K_{base} * \left(\overset{baseline}{H'_{roof} < H'_{room}} \right) \wedge (T'_{roof} > T'_{room}) + C_{base} \quad (15)$$

Finally, a slightly simpler control algorithm that only considers the absolute humidity but calculates a flow rate that is proportional to the difference between absolute humidity in the room and roof was tested. Dividing by the maximum difference between these absolute humidities ($\max(Q_{room} - Q_{roof})$) brings the output to within 0 and 1 so that scaling by K results in an output between 0 and the maximum measured flow rate:

$$QDiff = K * ((Q'_{room} - Q'_{roof}) > 0) * (Q'_{room} - Q'_{roof}) / \max(Q'_{room} - Q'_{roof}) \quad (16)$$

4. Results

4.1 Ventilation and airtightness survey

As described in section 3.1, the airtightness and ventilation of 36 randomly selected houses were examined over a 3–4 week period. N_{50} results for the 36 houses are shown in Figure 15. Figure 16. shows the effect from sealing all ventilation and obvious leakage openings.

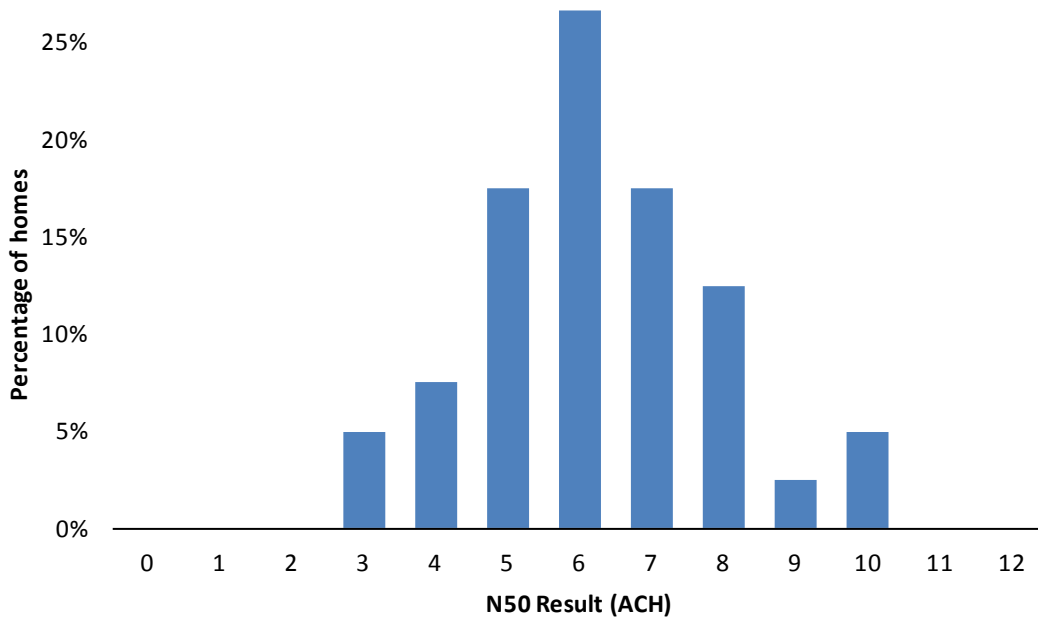


Figure 15. Distribution of airtightness measurements for post-1994 homes.

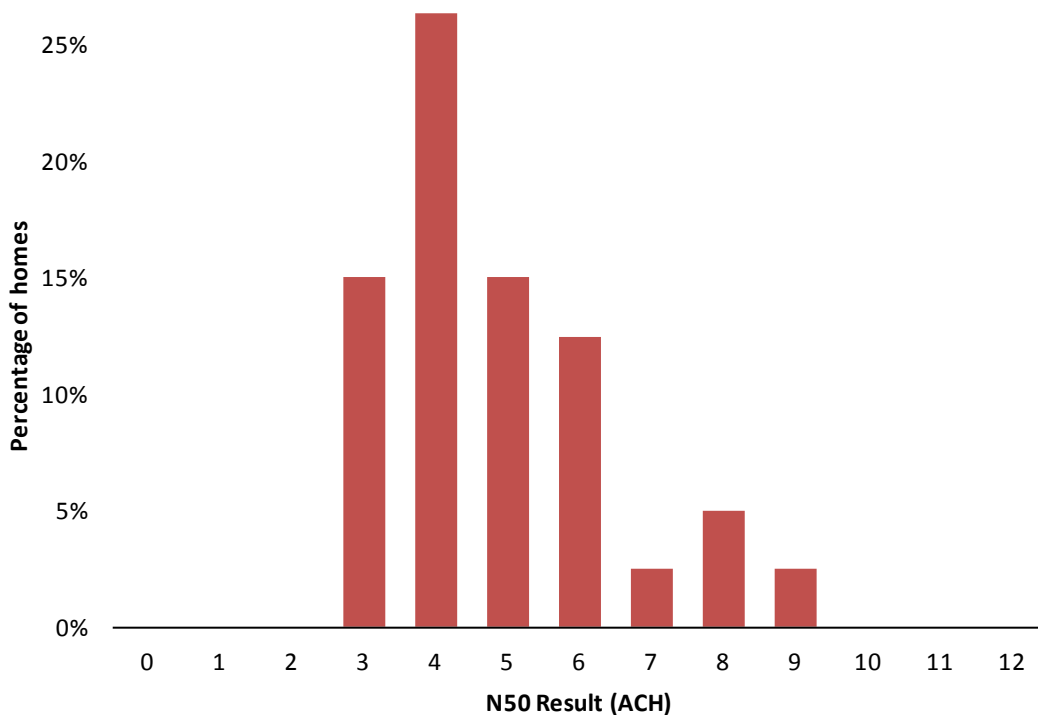


Figure 16. Distribution of airtightness results, with specific ventilation and obvious leakage openings sealed.

The results of the ventilation survey are plotted in Figure 17. against the estimated rate from the airtightness measurements made using Equation (1). Circled on the right are several outliers, three of which had a supply-only roofspace-sourced ventilation system. A line of slope 1 is also plotted.

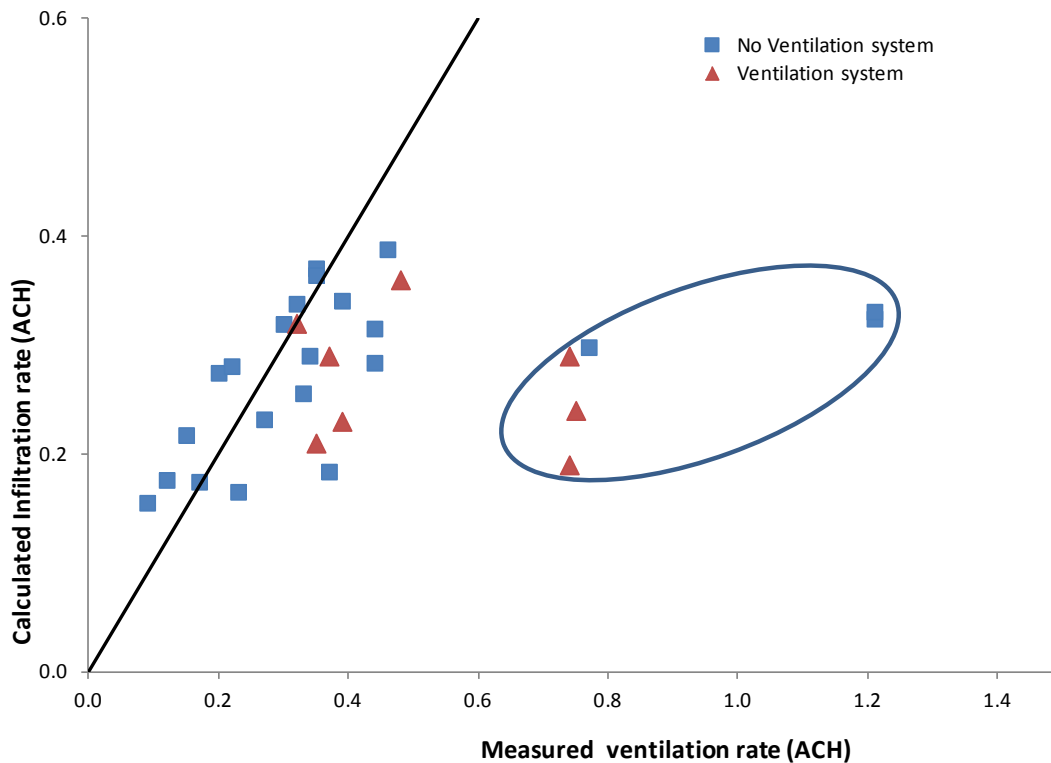


Figure 17. Infiltration versus measured ventilation, with outliers circled. Note that flow rates are given as air changes per hour at atmospheric pressure.

The most important change from the earlier surveys was the significant reduction in the mean N_{50} result from 8.5 ACH to 6.7 ACH. The mean floor area of the newer houses was also bigger than those in the last survey, increasing from 115 m² to 155 m² (not including internal-access garages). The recent N_{50} results also fell in a much tighter range (7.8–3.1 ACH), suggesting more consistency in construction.

Much of the difference between Figure 15. and Figure 16. was due to the leakage under internal-access garage doors. On average, a drop in the N_{50} result of 1.4 ACH was noted when the internal access for the garage spaces was sealed from the rest of the house. Internal garage doors therefore present an opportunity for increasing airtightness and reducing infiltration from an unheated (and potentially polluting) part of the building.

There are clearly two groups of houses in Figure 17. – those where the estimated infiltration rate and the measured ventilation rate are similar (25 cases) and those (six cases) where additional ventilation (either from opening windows or supply-only ventilation systems) has been provided.

In the larger group, the small difference between the estimated infiltration rate (0.28 ACH @ atmospheric pressure) and the measured ventilation rate (0.32 ACH @ atmospheric pressure) indicates limited window opening by the occupants over the period. The measured ventilation rate of 0.32 ACH @ atmospheric pressure sits at the lower end of guidelines for acceptable indoor air quality (Limb, 2001).

In addition, observations of the presence of mould and mildew were made at several of the homes studied – evidence of excess indoor moisture.

The PFT technique is a longer-term, time-averaged measurement method and thus does not lend itself well to resolving small, short-term changes in ventilation performance. However, it is clear that window opening and the operation of extract systems in bathrooms and kitchens has added less than 0.2 ACH @ atmospheric pressure on top of the background air infiltration in most of these houses.

Overall, there is limited evidence that windows are being opened often enough to provide the ventilation needed to control moisture and provide good indoor air quality in much of the sample presented here.

Eight homes in Figure 17. were fitted with supply-only ventilation systems. Three of these systems were shown to substantially increase ventilation above background infiltration to around 0.7 ACH @ atmospheric pressure. In the other five cases, little additional ventilation was provided by systems, several of which were apparently turned off to save energy during the period of PFT measurements.

4.2 Infiltration measurement

Infiltration rates were determined for the test house using tracer gas techniques (described in section 3.2.1) at various airtightness configurations. This was carried out in order to determine the infiltration techniques of the house before adding a ventilation system. Figure 18. and Figure 19. show the hourly averaged infiltration measurements of a single zone, i.e., one tracer gas over 2–4 days at different airtightness levels. The measurements were completed during a calm period with average wind speeds of only 2 m/s measured at 10 metres height.

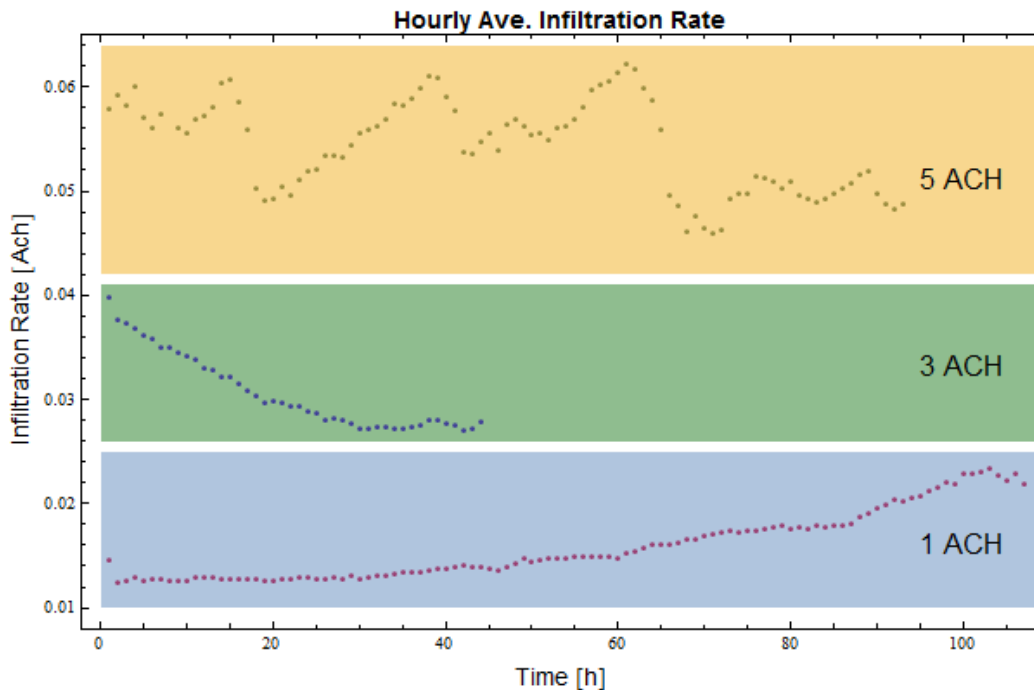


Figure 18. Single-zone infiltration rate of the living area at different N_{50} airtightness levels. The graph for the airtightness level of 9 ACH is provided separately due to its increased scale (see Figure 19.).

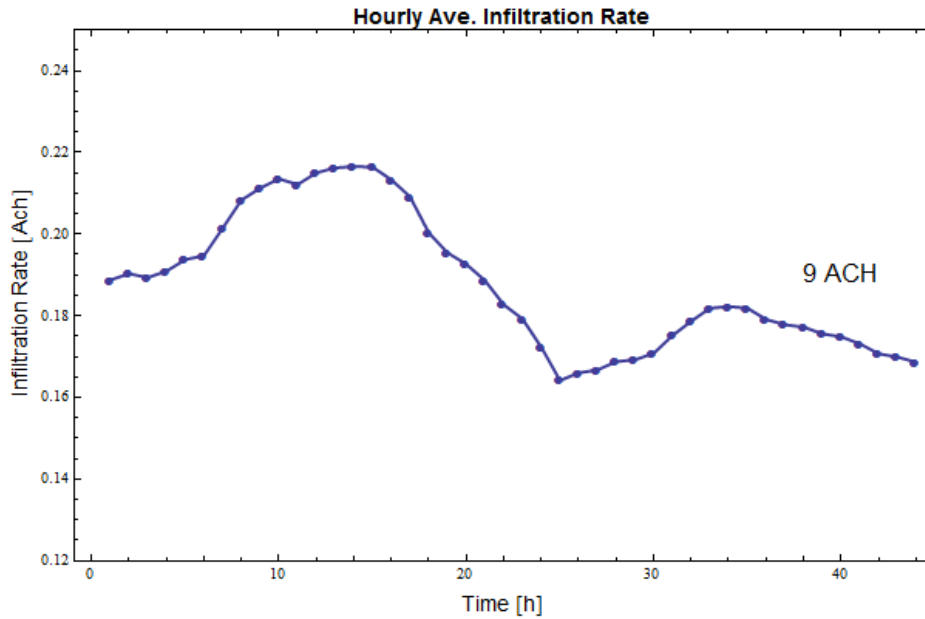


Figure 19. The graph shows the single-zone infiltration rate of the living area at about 9 N₅₀. All ports are open at this level of airtightness, but windows and doors are closed.

The hourly averaged infiltration rate of a short two-zone infiltration experiment is shown in Figure 20. One of the bedrooms (Zone 2 in Figure 9.) of the house was filled with CO₂, while the remaining living area (Zone 1 in Figure 9.) of the house was filled with SF₆. Both zones were at an airtightness level of about 2 ACH @ 50 Pa. Only wall ports were open during this experiment, therefore, there was no cross-infiltration between the two zones via the roof apart from through adventitious openings. Most of interzonal infiltration would have taken place through openings under the closed door. The average wind speed during this period was about 1.5 m/s at a height of 10 metres.

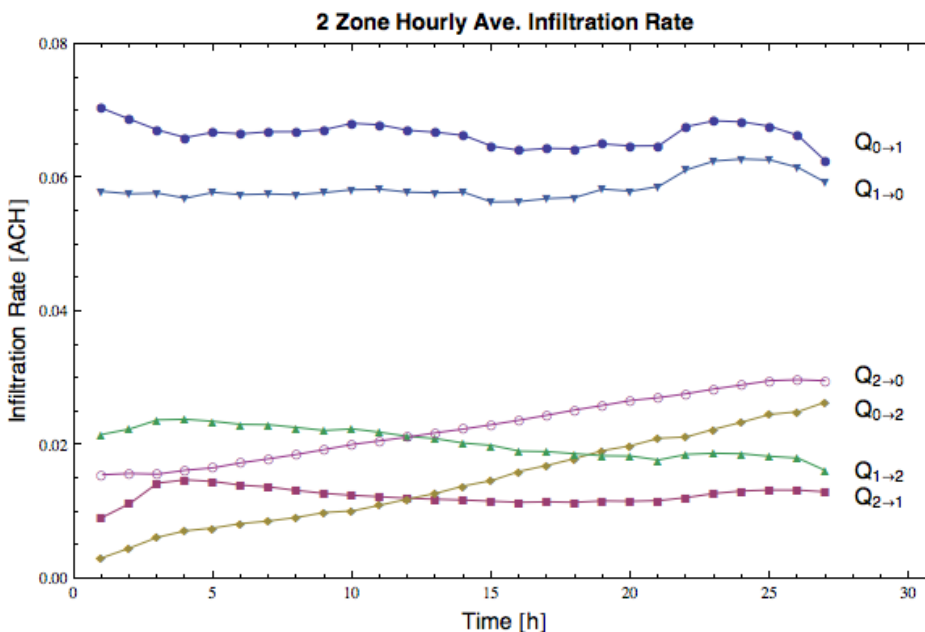


Figure 20. Infiltration rates for the two zones described in Figure 9. The legend shows the direction of flow (Q) for each line, where Zone 1 is denoted by the subscript 1, Zone 2 is denoted by subscript 2 and outside is denoted by subscript 0.

4.3 Tracer gas mixing experiments

As described in section 3.2.5, we investigated the mixing of tracer gas within the test house. This was carried out in the vertical and horizontal plane both in a north and south-facing zone of the building.

4.3.1 Vertical mixing

Figure 21 shows the difference in tracer gas concentration between three different heights above the zone floor for the two zones of interest (described in section 3.2.5) together with the relevant environmental data. We observed negligible variation between tracer gas concentrations at different heights for the two zones. The airtightness of each zone was approximately 1 ACH @ 50 Pa, with major changes in infiltration rate being wind driven. For the majority of the two experiments, wind speed was less than 4 ms^{-1} , with no discernible impact on the vertical mixing of the tracer gas (McDowall and Plagmann, 2014).

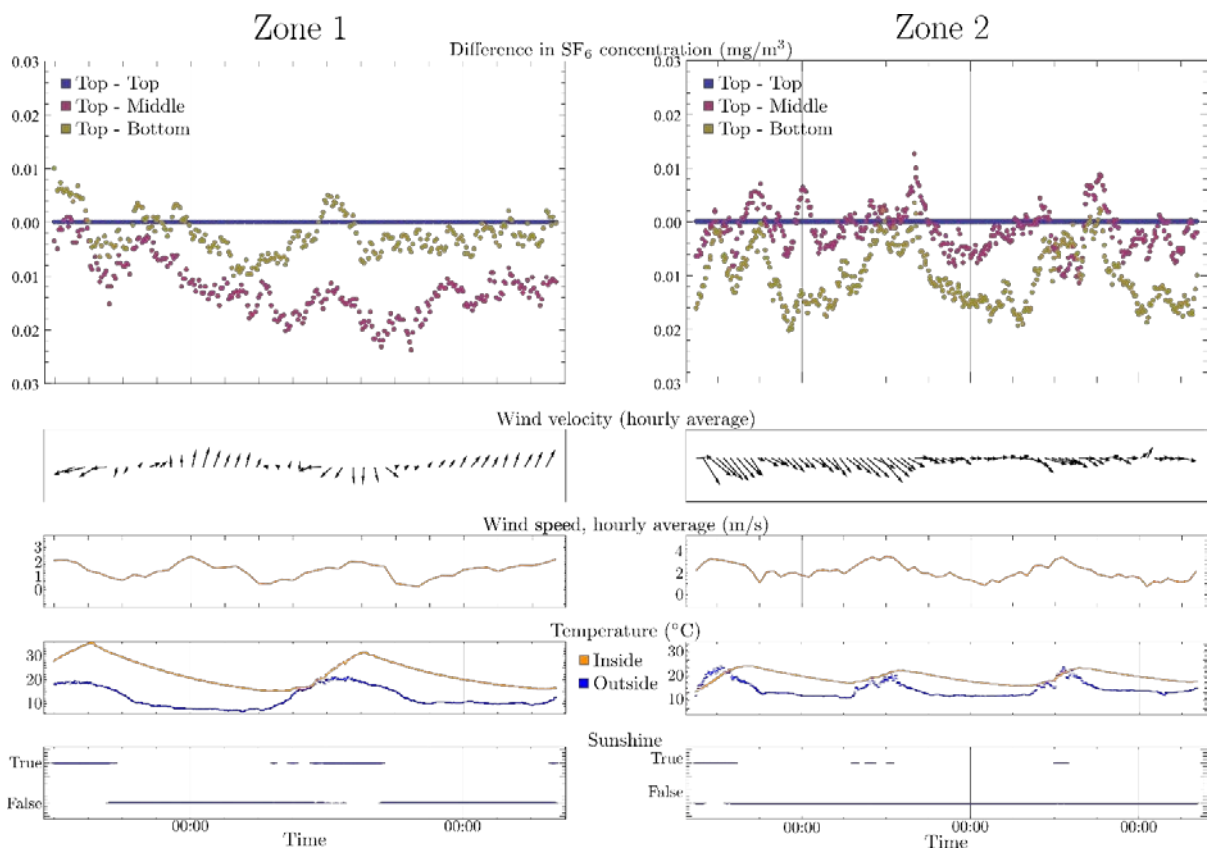


Figure 21. Results of vertical mixing experiment for Zones 1 and 2. Three sample points were used – 2065 mm (top), 1065 mm (middle) and 55 mm (bottom) above the zone floor. The two uppermost plots show the difference in SF₆ concentration between the top sample point and the middle and bottom sample points.

4.3.2 Horizontal mixing

Figure 22. shows the difference in tracer gas concentration between four different locations of equal height in each of the two zones together with the relevant environmental data. Zone 1 shows no discernible variation between tracer gas concentrations at the different sampling locations, suggesting good mixing in that zone.

A discrepancy between gas concentrations at different sampling points in Zone 2 indicated incomplete mixing within that zone. This feature appears more prominently at certain times of the day when tracer gas concentrations are greater at the southernmost sampling points than at the northernmost sampling points in the room.

The airtightness of Zones 1 and 2 during the horizontal mixing experiments was approximately 8 ACH @ 50 Pa. Both zones were measured over periods that had similar wind velocities and sunshine hours. However, we do note that the ambient air temperature inside the zone was on average warmer in Zone 1 than in Zone 2. This discrepancy was expected since Zone 1 is north-facing whereas Zone 2 faces away from the sun.

The infiltration rate of a given zone can be determined from the general mass balance equation given by Equation (2). Using this expression and the concentration data for horizontal mixing in Figure 22, we were able to estimate the error associated with an infiltration measurement under the current conditions. We did this by first determining the infiltration rate based on the concentration data from each sampling point individually averaged over 24 hours. We considered the true infiltration rate to be the mean of the four values (one for each sampling point) with an error given by the standard deviation.

Incomplete mixing in Zone 2 in the horizontal plane was found to give an uncertainty in the infiltration measurement of approximately 4%. This is in comparison to the same experiment in Zone 1 that displayed good tracer gas mixing, where we found the infiltration rate uncertainty to be approximately 1%.

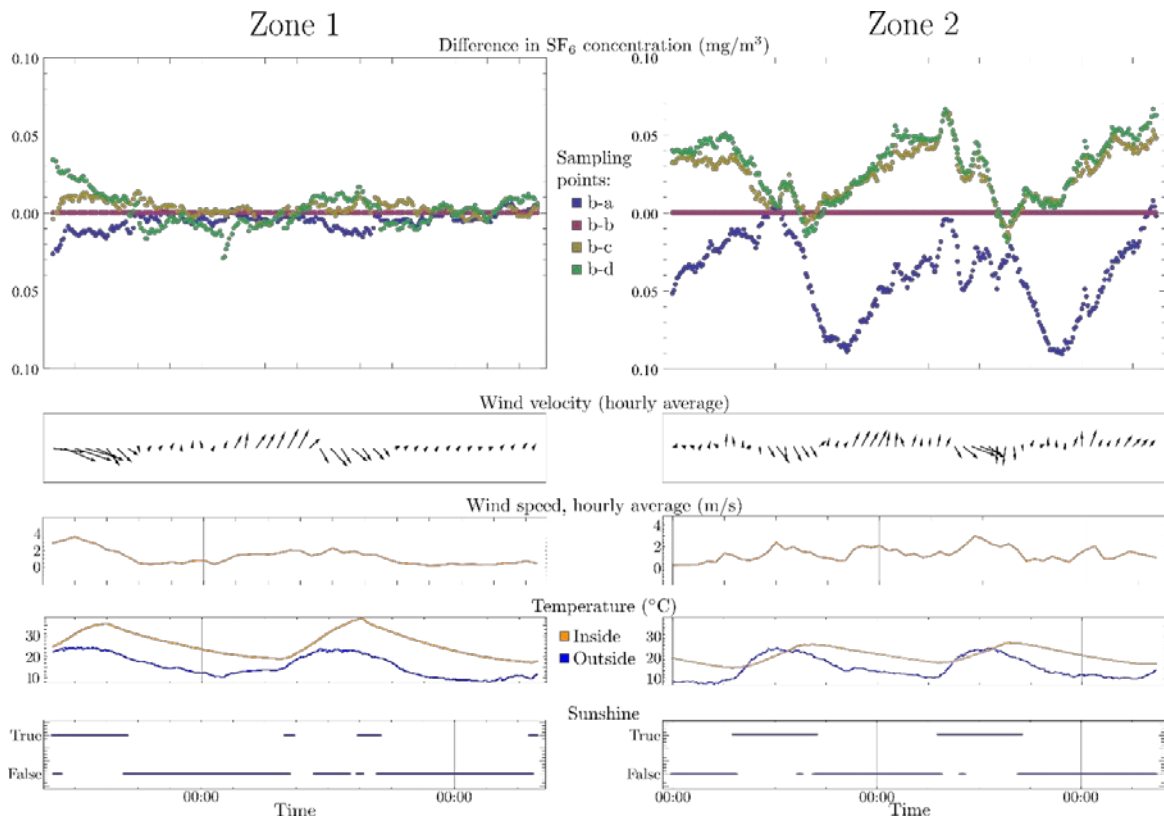


Figure 22. Results of horizontal mixing experiment for Zones 1 and 2. Four sampling points were used in each zone as illustrated in Figure 8. A consistent SF₆ concentration across all sampling points in Zone 1 indicates good mixing in the horizontal plane within that zone. Variation in tracer gas concentration at different sampling points in Zone 2 suggests incomplete mixing within that zone.

Discussion

The tracer gas appeared to mix reasonably well in the vertical plane for both the north-facing zone (Zone 1) and south-facing zone (Zone 2) regardless of external environmental conditions. The same conclusions can also be drawn for horizontal mixing in the north-facing zone. However, horizontal mixing in the south-facing zone appears to suffer from stratification at certain times of the day. This stratification leads to a greater uncertainty when determining the infiltration rate and, as such, is an issue that deserves consideration.

The collective mixing effects of diffusion, convection, direct solar radiation convection and air movement through infiltration all contribute to mixing of a tracer gas within a zone. The two zones we considered were of roughly equal airtightness and tested under similar environmental conditions.

From this, it can be concluded that direct solar radiation was the limiting mechanism for mixing. In the south-facing zone, where incomplete tracer gas mixing was observed, there was no direct solar radiation into the zone, which is in contrast to the north-facing zone.

Convections within a zone can be driven by temperature gradients caused by solar radiation. Air within a zone can absorb heat when in contact with direct solar radiation through, say, a window. Buoyancy forces cause the warm air to rise due to the stack effect (Straube et al., 1995), creating a convective process as cold air moves to fill the void left by the warm air. This convective process increases mixing of the tracer gas with the air present in the zone. The absence of direct solar radiation in Zone 2 meant the occurrence of this process was minimal, leading to incomplete mixing.

It has been assumed here that the stack effect is the dominant source of natural mixing within the zone. However, it should be noted that a less airtight house or one that is more susceptible to wind-driven ventilation (for example, in an area of greater wind speeds) may have enough natural ventilation to adequately mix all the air within the zone and hence not exhibit the same behaviour observed here.

The magnitude of infiltration rate errors resulting from incomplete mixing are due partly to the geography of the zone being measured and the ventilation within it. Van Buggenhout et al. (2009) observed an error of 86% between the measured and the actual ventilation rate for a mechanically ventilated test zone with openings at each end. Tracer gas concentration differences of up to 44% have been observed within a single zone of a three-storey test house (Maldonado et al., 1983).

Both of these experiments were performed under different conditions to the experiments presented here and therefore do not allow for direct comparison of errors. However, they do show that incomplete tracer gas mixing is not a feature specific to just our test building.

In conclusion, a lack of direct solar radiation can lead to incomplete mixing of a tracer gas within a zone when no artificial mixing apparatus is used. It was shown that, for the test house used in our experiments, this incomplete mixing caused an increase in the uncertainty of our infiltration measurements from approximately 1% in a sun-facing zone to 4% in a non-sun-facing zone in the horizontal plane. Tracer gas concentrations in the vertical plane were observed to display good mixing in both zones.

4.4 Ventilation measurements – two zone

As described in section 3.2.6, a comparison was made between the variability of infiltration and ventilation rates across different airtightness levels in the test house. This was carried out using two zones over 2 consecutive years both with and without the supply-only ventilation system running.

Year 1

Figure 23. and Figure 24. show the total mean ventilation rates in each zone for year 1, for the infiltration-only and ventilated cases respectively. As stated in section 3.2.6, there were ports opened to achieve the spread of airtightness levels, and year 1 included some ceiling ports.

Error bars on the plots indicate the standard deviations of the dataset. As expected, there is a steady trend to lower flows as the airtightness increases (Figure 23.). This is in contrast to the flows measured with the supply-only ventilation in Figure 24.

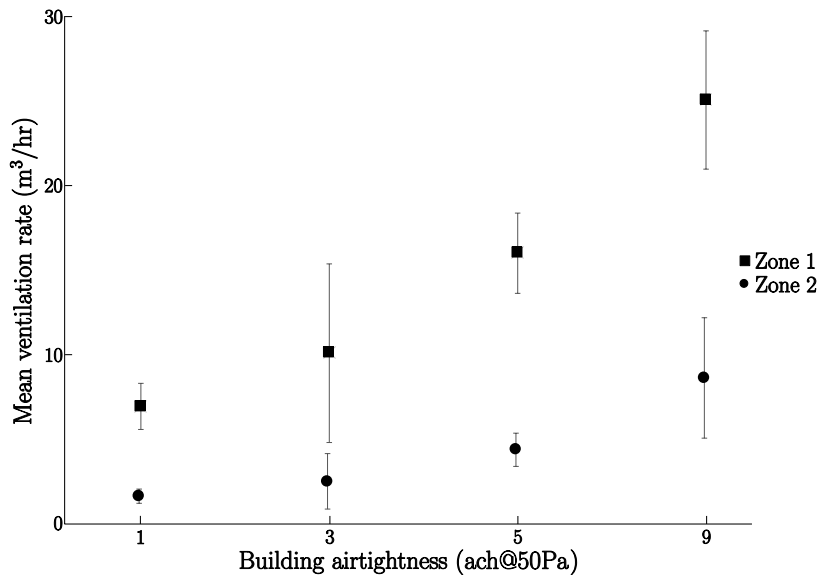


Figure 23. Mean total ventilation rates for each zone versus airtightness – infiltration only.

The supply-only ventilation system was switched on and the diffusers uncovered in late May 2012. Figure 24. presents the averaged calculated flows for each of the zones across the different airtightness levels.

As expected, average flows for each zone are substantially higher than the infiltration-only case. However, there does not appear to be a clear trend with building airtightness – just slightly more variation in the rates.

This can be explained by the control algorithm for the ventilation system switching on an off as the temperature difference between the roofspace and the living space varied.

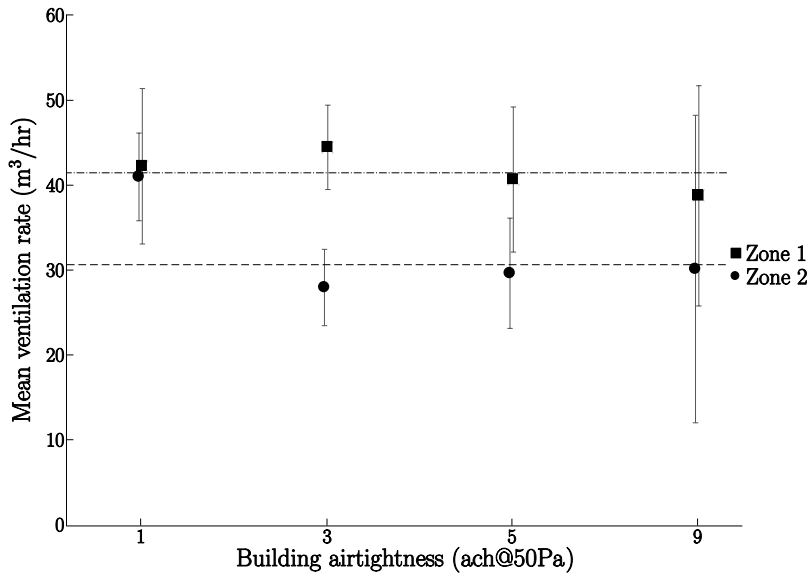


Figure 24. Mean ventilation rates for each zone versus airtightness – supply-only ventilation.

Figure 25 shows the amount of airflow between zones in the infiltration-only case for the range of airtightness levels of the test building (1, 3, 5 and 9 ACH @ 50 Pa). Each flow is averaged over several days of measurements, and the standard deviations of each dataset are represented by the error bars.

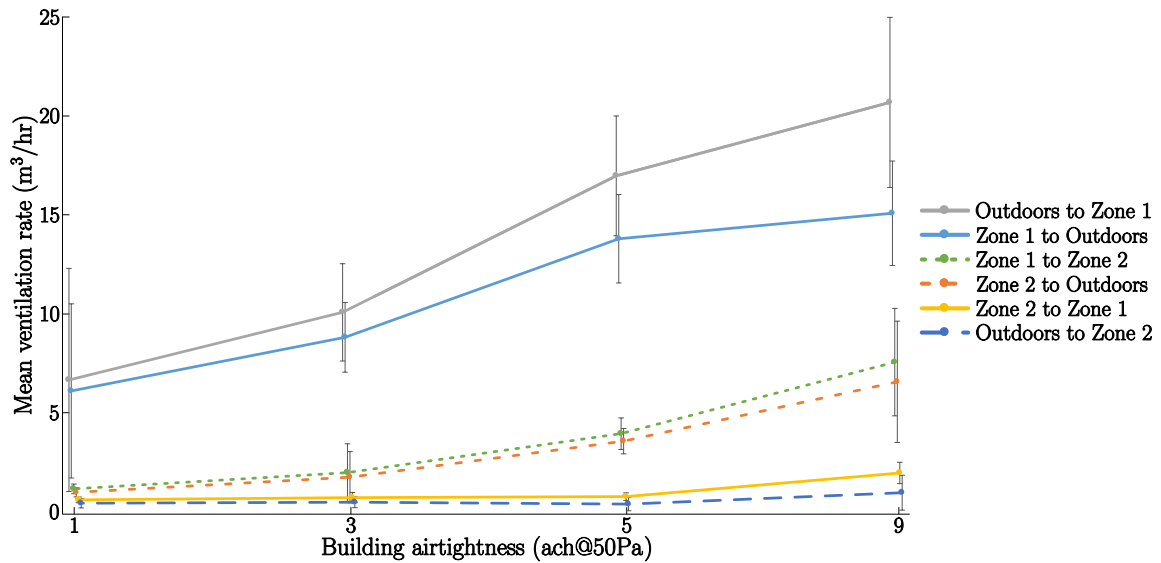


Figure 25. Interzonal ventilation rates for each zone versus airtightness – infiltration only – year 1.

Year 2

The experiments above were repeated for a second winter, but with three important differences:

- No ceiling ports were opened during the experiments.
- The supply-only ventilator ducts were only open to Zone 2, so no active ventilation took place in Zone 1.
- The default control system for the ventilation system was not used – a simple constant rate was applied.

The exclusion of the ceiling ports limited recirculation of exfiltrated room air back to the room due to the ventilation system, and it limited the minimum airtightness that could be achieved in practice (6.5 versus 9 ACH @ 50 Pa).

Results of these are shown below in Figure 26. and Figure 27.

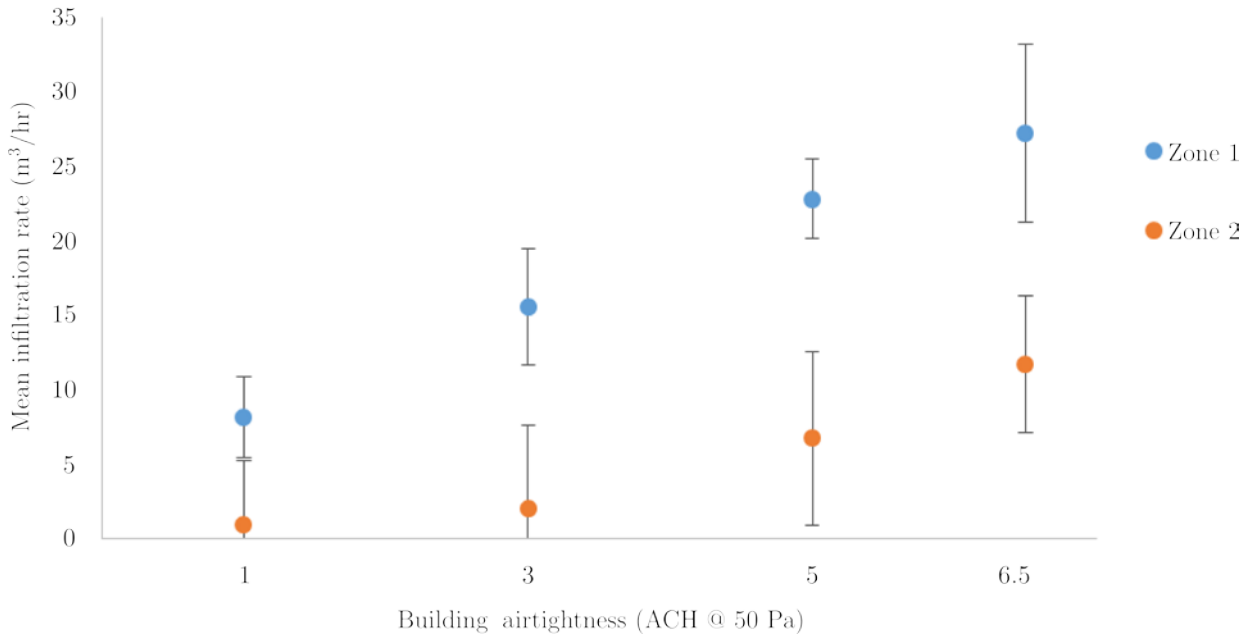


Figure 26. Infiltration only – year 2.

As can be seen in Figure 26., very similar results were achieved for the infiltration-only case from year 1 shown in Figure 23.

In Figure 27., there is a more even level of ventilation measured in the building, due to the fan being set to a constant output. Again, the variation due to varying airtightness of the building is quite low, indicating the dominance of the mechanical system over the natural driving forces.

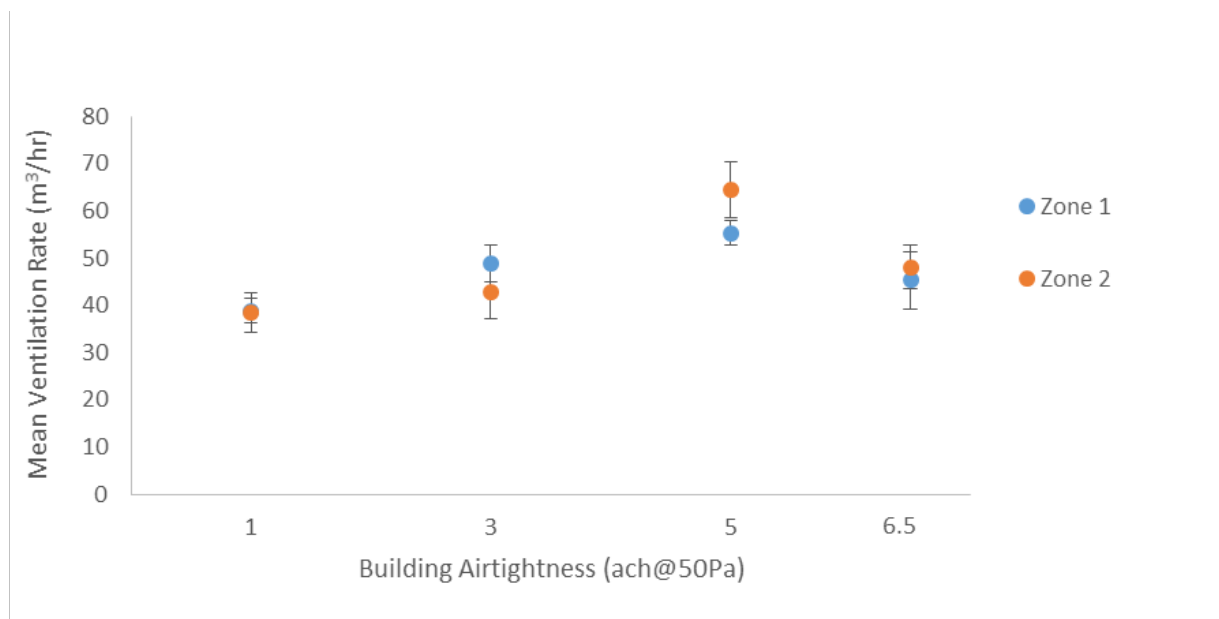


Figure 27. Ventilation rate with supply-only ventilation – year 2.

Discussion

As expected, the ventilation rate measurements for the infiltration-only cases show a lack of air exchange on average – this applies for both year 1 and year 2. Even with the building configured for 9 ACH @ 50 Pa in year 1, the mean total flows for Zones 1 and 2 are 25.1 m³/hr (equivalent to 0.13 ACH @ atmospheric pressure) and 8.7 m³/hr (0.39 ACH @ atmospheric pressure) respectively. Though this may look as though Zone 2 is getting sufficient ventilation, from Figure 25, it is apparent that much of the air entering Zone 2 is coming via Zone 1, not from outdoors. This is a common trend in the infiltration-only case.

The reason for Zone 2 being essentially a transit point for air en route to outdoors has been identified as Zone 2 being on the leeward of the prevailing wind direction, causing a low pressure zone in that corner of the house driving the air out of the house.

Since Zone 1 is ventilated to a low level, it brings into question the quality of the air ventilating Zone 2, which highlights one of the biggest difficulties with infiltration make-up air. One is never certain of the source of this air.

The ventilation measurements for the supply-only ventilation case are shown to be much higher on average than infiltration only. Results for year 1 indicate an overall mean for Zone 1 of 41.6 m³/hr (0.23 ACH @ atmospheric pressure) and Zone 2 of 32.2 m³/hr (0.68 ACH @ atmospheric pressure).

The average results do not show a visible trend with airtightness of the envelope. However, the influence of increasing infiltration and the control system of the ventilation system is evident as the standard deviation of the measurements gets larger as the building becomes less airtight. It is likely here that the infiltration component is becoming significant enough to influence the overall ventilation to a minor extent.

From Figure 23. and Figure 26., it is clear that infiltration alone cannot be expected to provide a significant amount of make-up air as New Zealand buildings get more airtight. Supplemental ventilation is therefore necessary if occupants do not open windows as often as the Building Code assumes.

The work described in section 4.1 suggests that window opening cannot be relied on in a significant number of homes. Addition of a ventilation system (whether supply only or balanced) may be a solution for some homeowners. However, control of any system will be an issue, particularly considering the indoor/outdoor lifestyles of many New Zealanders during warmer months.

4.5 CONTAM modelling

4.5.1 Single-zone infiltration model

In this study, CONTAM was used to model the infiltration of the simple single-zone test building at different airtightness levels. Each model is compared to the empirical data obtained from the experimental building described above. Four CONTAM models were created to simulate the four different levels of airtightness tested using the experimental building described above – 1, 3, 5 and 9 ACH @ 50 Pa. Environmental conditions such as temperature and wind velocity measured during each empirical experiment were used as input parameters for the CONTAM simulation corresponding to the same airtightness. In what follows, we present results of our simulations at each airtightness level and their comparison to the experimental data.

1 ACH @ 50 Pa model

Figure 28(a) shows the comparison between the measured infiltration rate for the experimental test building at 1 ACH @ 50 Pa and the infiltration rate determined using a CONTAM simulation. Due to the relatively high airtightness level and other variables such as sampling location, tracer gas mixing profile and wind direction, we observed a delay between changes in wind velocity and its effect on the infiltration rate. This effect, however, was not apparent in our CONTAM simulation because it assumes instantaneous, perfect mixing which did not occur in the test building. This delay was allowed for in our CONTAM model by convolving the output with a kernel in the form of an inverse Gaussian distribution. A convolution of the model was chosen over a deconvolution of the empirical data simply to keep the empirical data intact.

The solid curve in Figure 28(a) is the result of a convolution between the output of the CONTAM simulation and an inverse Gaussian distribution given by:

$$y = Ax^{\theta-1} \exp\left[\frac{-\lambda}{2x} \frac{x^2}{\mu^2+1}\right] \quad (17)$$

where $A = 530$, $\mu = 6$, $\lambda = 10$ and $\theta = 4$. This has the effect of shifting the CONTAM measured infiltration rate in time so as to account for the response delay observed in the experimental data. The multiplication factor A in Equation (17) was required because the convolution process altered the integral of the original curve. We used A to bring the integral of the convoluted curve to within <2% of the original curve.

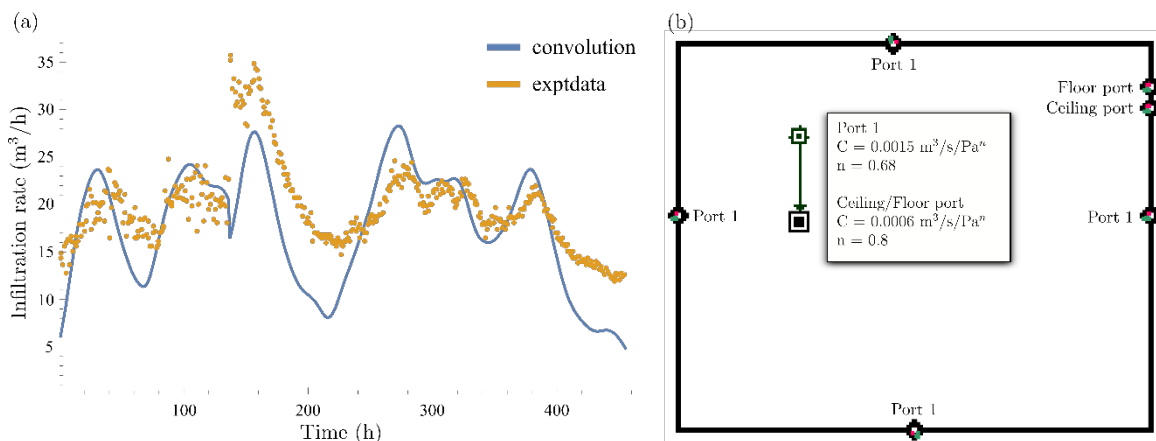


Figure 28. (a) Yellow dots = empirical measurement of the infiltration rate for the experimental test building at 1 ACH @ 50 Pa. Blue solid line = infiltration rate of experimental building determined using CONTAM simulation and a convolution. (b) Graphical representation of CONTAM model used to simulate the infiltration in (a).

1 ACH @ 50 Pa was the greatest airtightness we could achieve using the experimental building. That is to say it represents the uncontrollable background infiltration rate that is present for all our experiments. For this reason, we used the same basic 1 ACH model for all our modelling and simply added extra airflow paths when simulating less airtight houses.

3 ACH @ 50 Pa Model

Figure 29 shows the comparison between an experimentally obtained infiltration rate for the test house at 3 ACH @ 50 Pa and a CONTAM model made using the same weather data. The graphical representation of the CONTAM model is shown in Figure 29(b). Similar to the 1 ACH @ 50 Pa case described above, we observed a delay in the response of the empirically determined infiltration rate to changes in wind that was not

present in the CONTAM model. To account for this in our model, we convolved the output of the CONTAM model with a curve generated by Equation (17) with $A = 200$, $\mu = 6$, $\lambda = 8$ and $\theta = 3$.

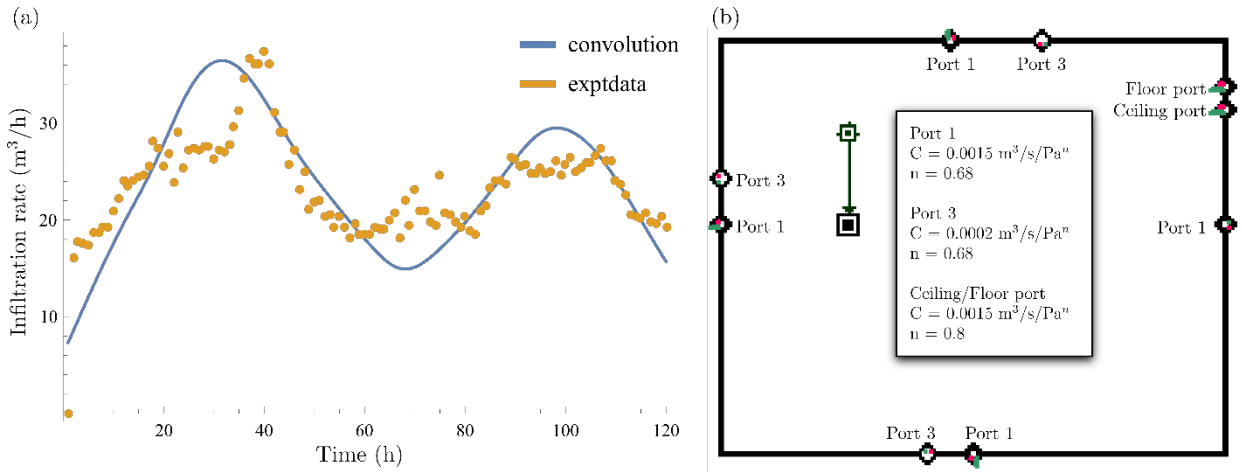


Figure 29. (a) Yellow dots = empirical measurement of the infiltration rate for the experimental test building at 3 ACH @ 50 Pa. Blue solid line = infiltration rate of experimental building determined using CONTAM simulation and a convolution. (b) Graphical representation of CONTAM model used to simulate the infiltration in (a).

5 ACH @ 50 Pa Model

Figure 30 shows the comparison between the experimentally obtained infiltration rate for the test house at 5 ACH @ 50 Pa and a CONTAM model made using the same weather data. The graphical representation of the CONTAM model is shown in Figure 30(b). Unlike the two models above, we did not use a convolution to correct for a delay in response time of the infiltration rate. This is because the airtightness of the test house is low enough at 5 ACH @ 50 Pa for the wind to have an immediate effect on the infiltration rate of the house.

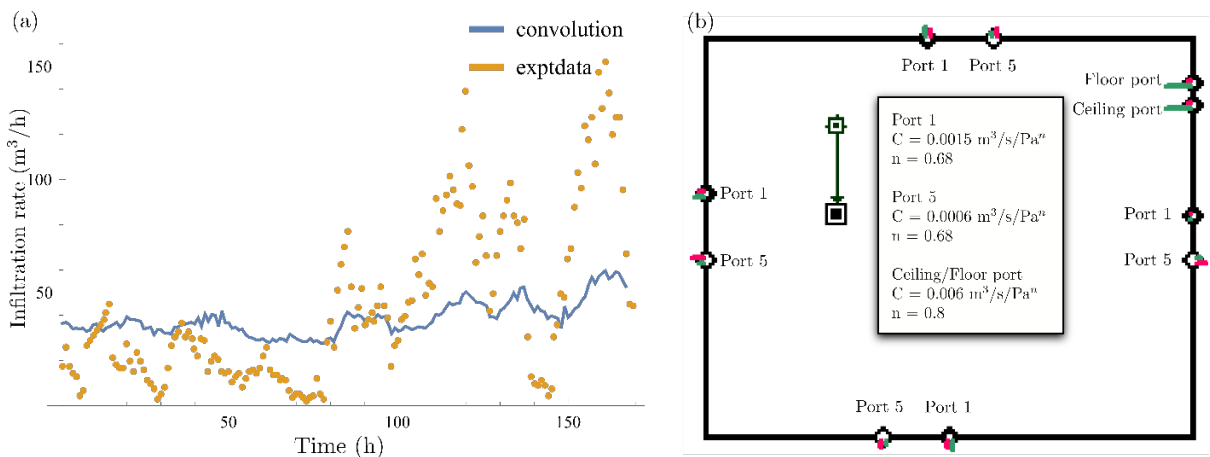


Figure 30. (a) Yellow dots = empirical measurement of the infiltration rate for the experimental test building at 5 ACH @ 50 Pa. Blue solid line = infiltration rate of experimental building determined using CONTAM simulation. (b) Graphical representation of CONTAM model used to simulate the infiltration in (a).

9 ACH @ 50 Pa Model

Figure 31. shows the comparison between the measured infiltration rate for the experimental test building at 9 ACH @ 50 Pa and the infiltration rate determined using a CONTAM simulation. Because of the relatively low airtightness of the test house at 9

ACH @ 50 Pa, wind effects on the infiltration rate were observed almost immediately, eliminating the need for a convolution.

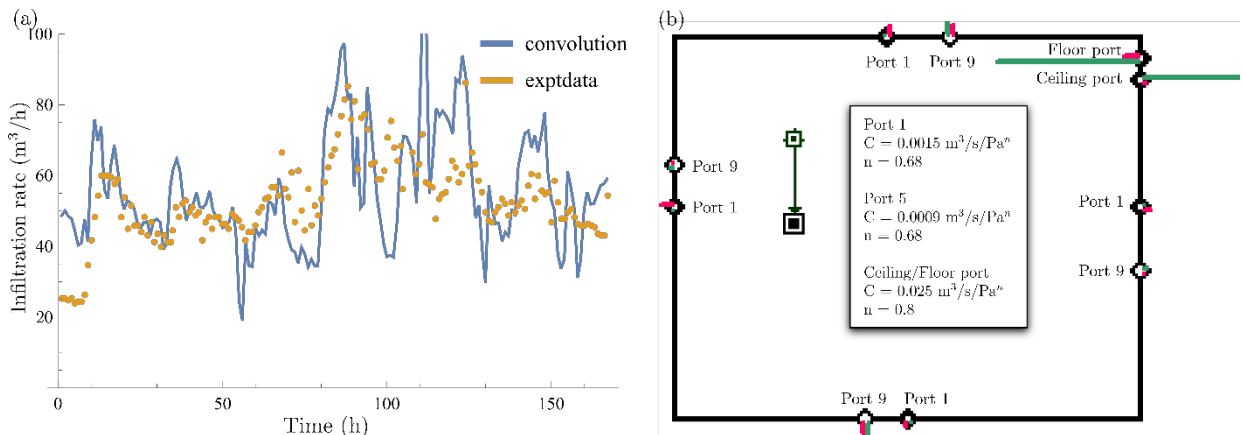


Figure 31. (a) Yellow dots = empirical measurement of the infiltration rate for the experimental test building at 9 ACH @ 50 Pa. Blue solid line = infiltration rate of experimental building determined using CONTAM simulation. (b) Graphical representation of CONTAM model used to simulate the infiltration in (a).

4.5.2 Infiltration in different cities

The four CONTAM models described in section 4.5.1 were used to model infiltration in different climate zones within New Zealand.

Each of the four airtightness levels (1, 3, 5, and 9 ACH @ 50 Pa) were run using typical yearly wind and temperature weather data (Liley et al., 2007) for six different cities/regions. The inside temperature was set to a constant 18°C and an urban wind zone assumed.

The six regions modelled were Northland, Auckland, Taupo, Wellington, Christchurch and Dunedin. The result is an indication of expected infiltration at different levels of airtightness for different places in New Zealand.

This can be used to help determine the level of extra ventilation required to manage typical moisture loads inside New Zealand homes around the country.

For each of the following figures the output of the CONTAM model is shown in blue with units of air changes per hour at atmospheric pressure. The average infiltration rate of the CONTAM model output is given by a yellow line. A light green band is used to illustrate the range of minimum ventilation rates amongst countries that specify a minimum rate with the ASHRAE recommended standard given in orange (ASHRAE Standard 62.2, 2007).

Northland

Figure 32. shows the typical yearly infiltration rate for a single-zone house in Northland at different airtightness levels. The 1 and 3 ACH models both used a convolution with an inverse Gaussian distribution as described in section 4.5.1.

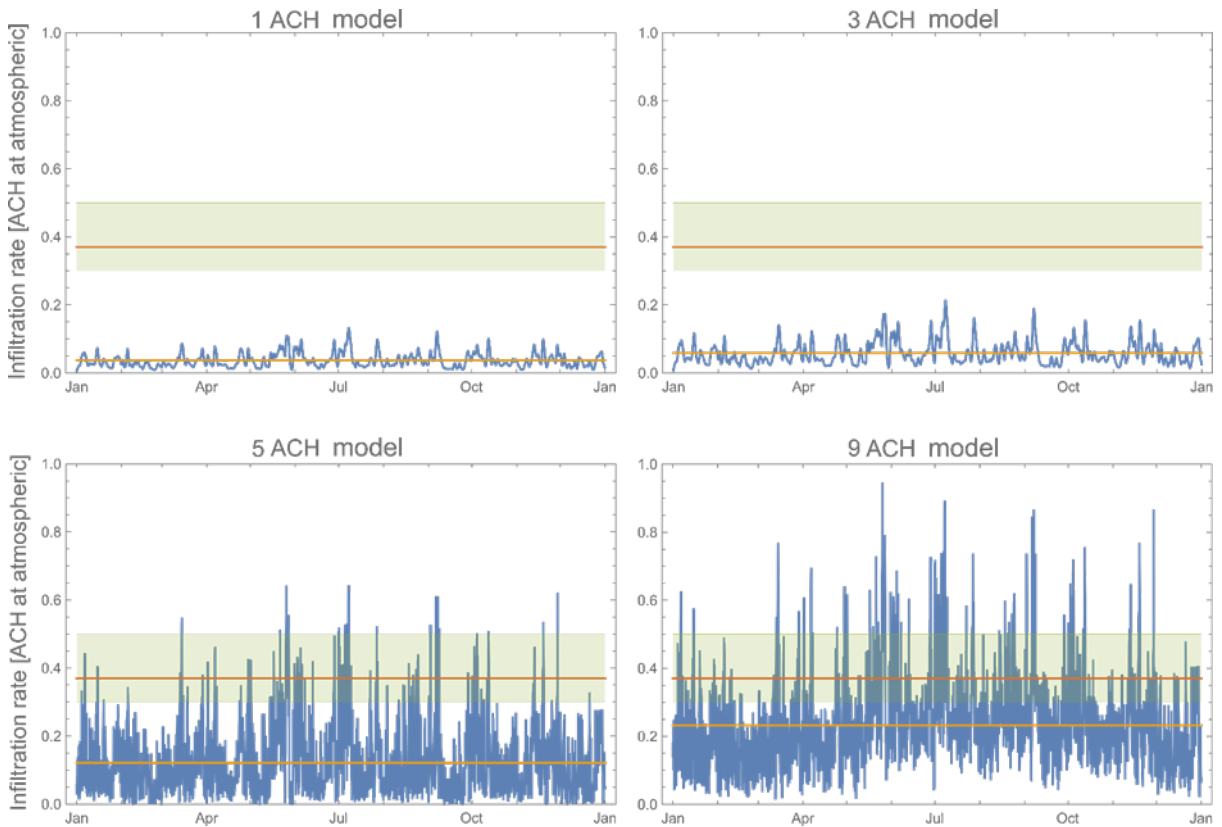


Figure 32. Infiltration model for a single-zone Northland house at various airtightness levels.

Auckland

Figure 33 shows the typical yearly infiltration rate for a single-zone house in Auckland at different airtightness levels. The 1 and 3 ACH models both used a convolution with an inverse Gaussian distribution as described in section 4.5.1.

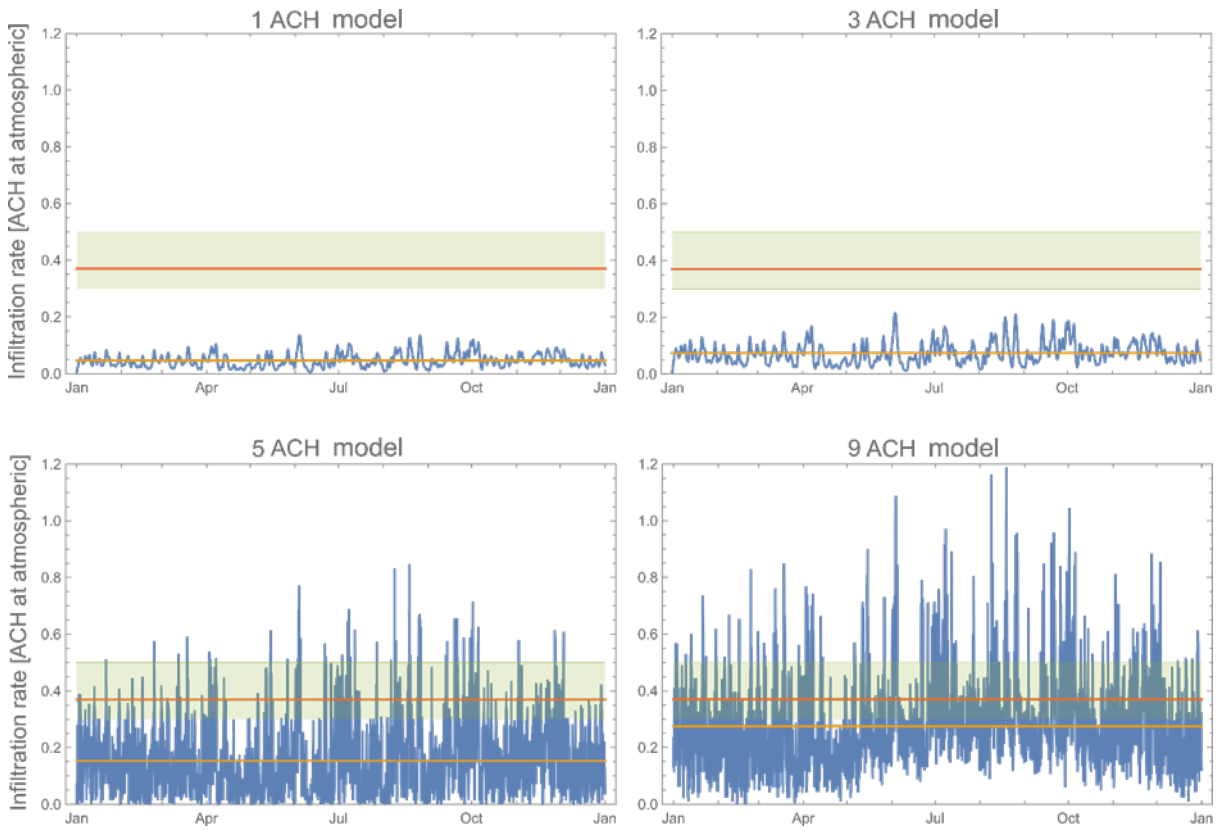


Figure 33. Infiltration model for a single-zone Auckland house at various airtightness levels.

Taupo

Figure 34. shows the typical yearly infiltration rate for a single-zone house in Taupo at different airtightness levels. The 1 and 3 ACH models both used a convolution with an inverse Gaussian distribution as described in section 4.5.1.

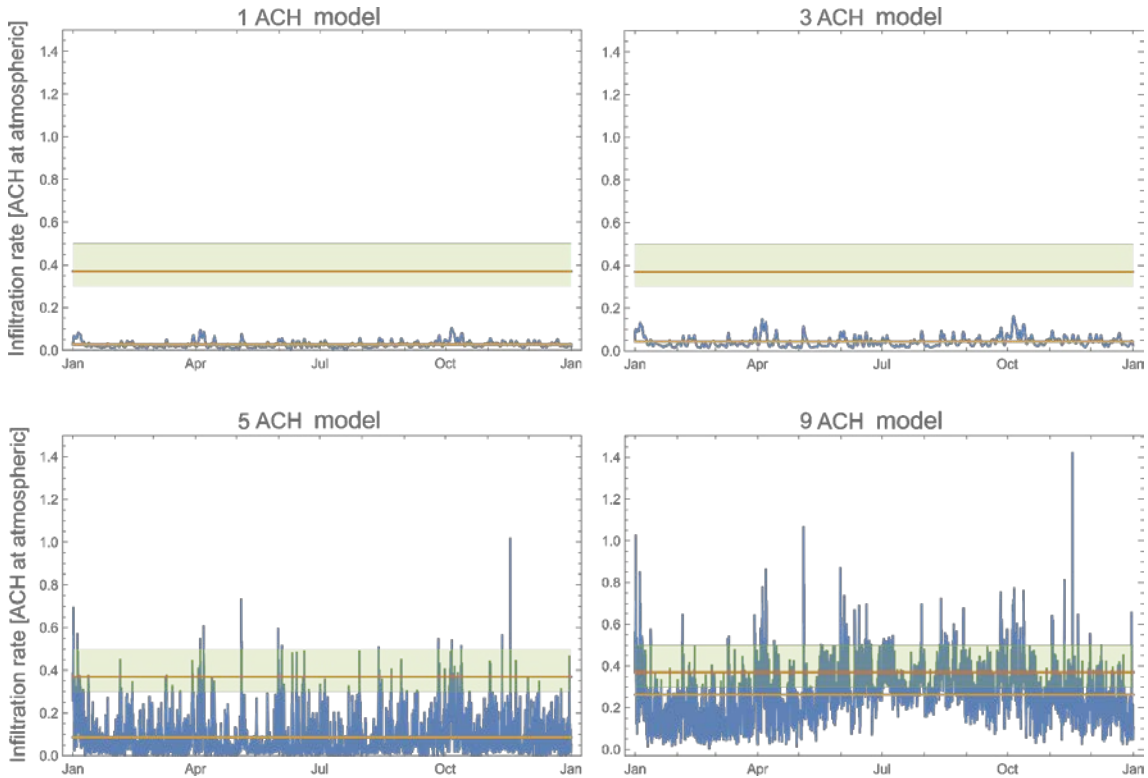


Figure 34. Infiltration model for a single-zone Taupo house at various airtightness levels.

Wellington

Figure 35 shows the typical yearly infiltration rate for a single-zone house in Wellington at different airtightness levels. The 1 and 3 ACH models both used a convolution with an inverse Gaussian distribution as described in section 4.5.1.

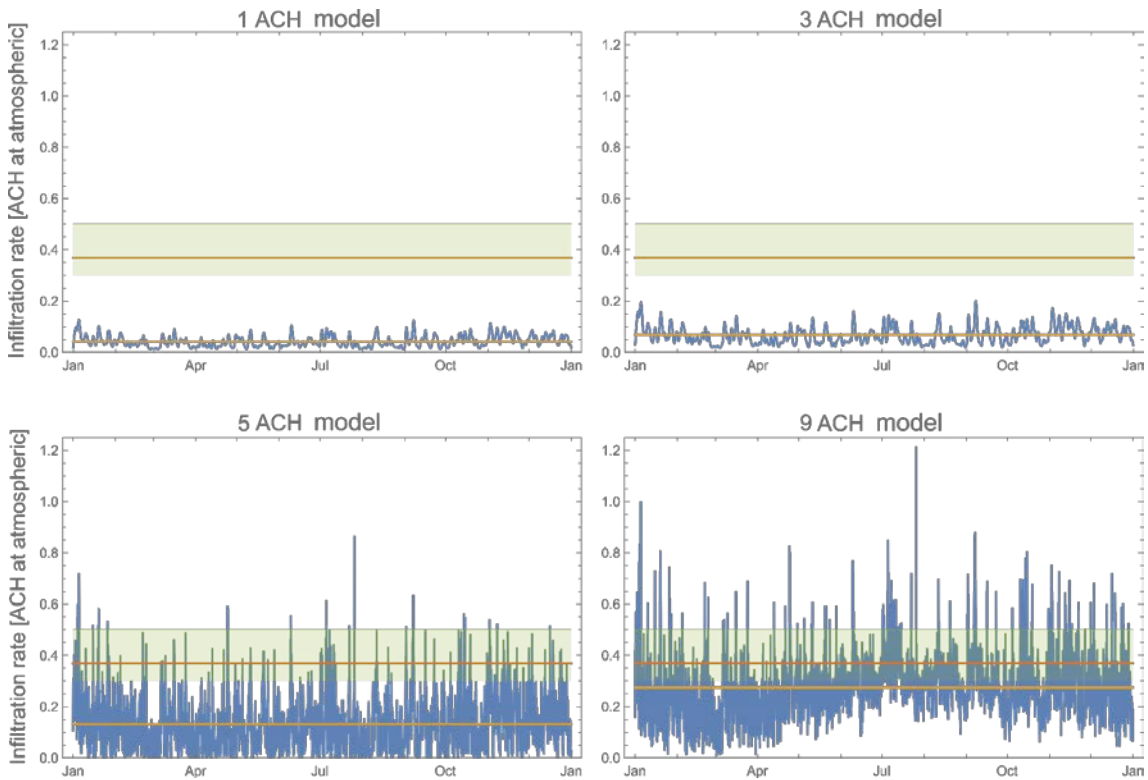


Figure 35. Infiltration model for a single-zone Wellington house at various airtightness levels.

Christchurch

Figure 36. shows the typical yearly infiltration rate for a single-zone house in Christchurch at different airtightness levels. The 1 and 3 ACH models both used a convolution with an inverse Gaussian distribution as described in section 4.5.1.

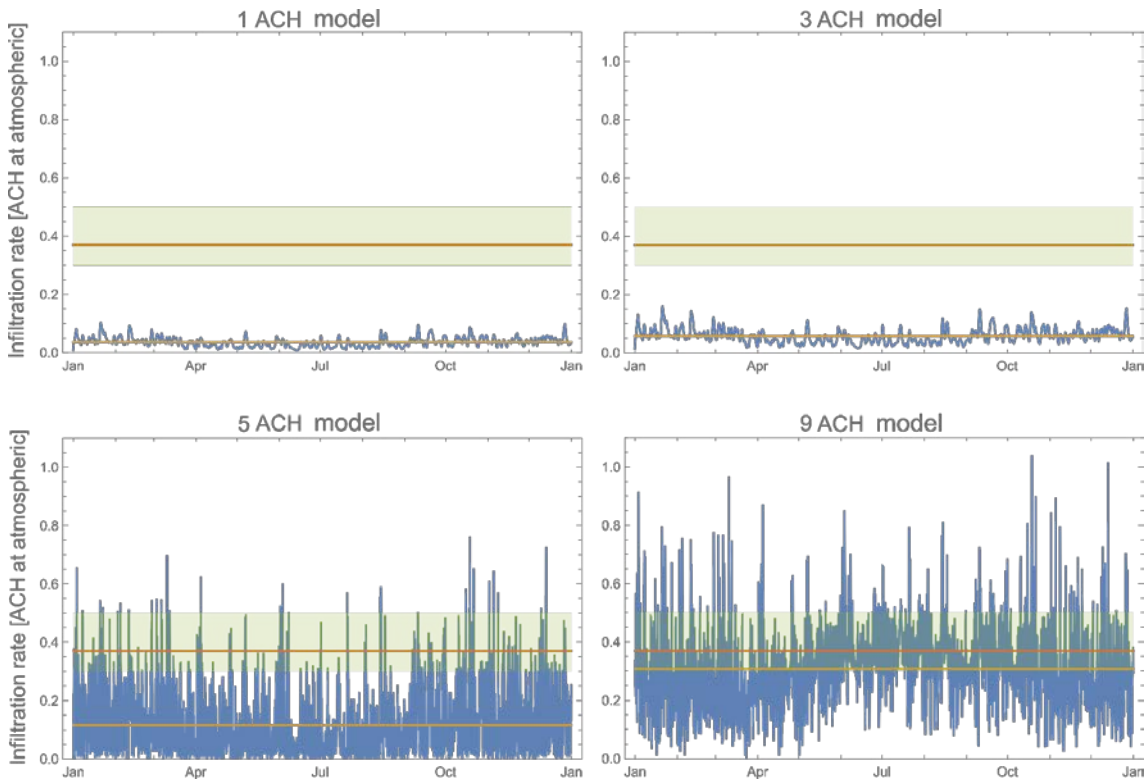


Figure 36. Infiltration model for a single-zone Christchurch house at various airtightness levels.

Dunedin

Figure 37. shows the typical yearly infiltration rate for a single-zone house in Dunedin at different airtightness levels. The 1 and 3 ACH models both used a convolution with an inverse Gaussian distribution as described in section 4.5.1.

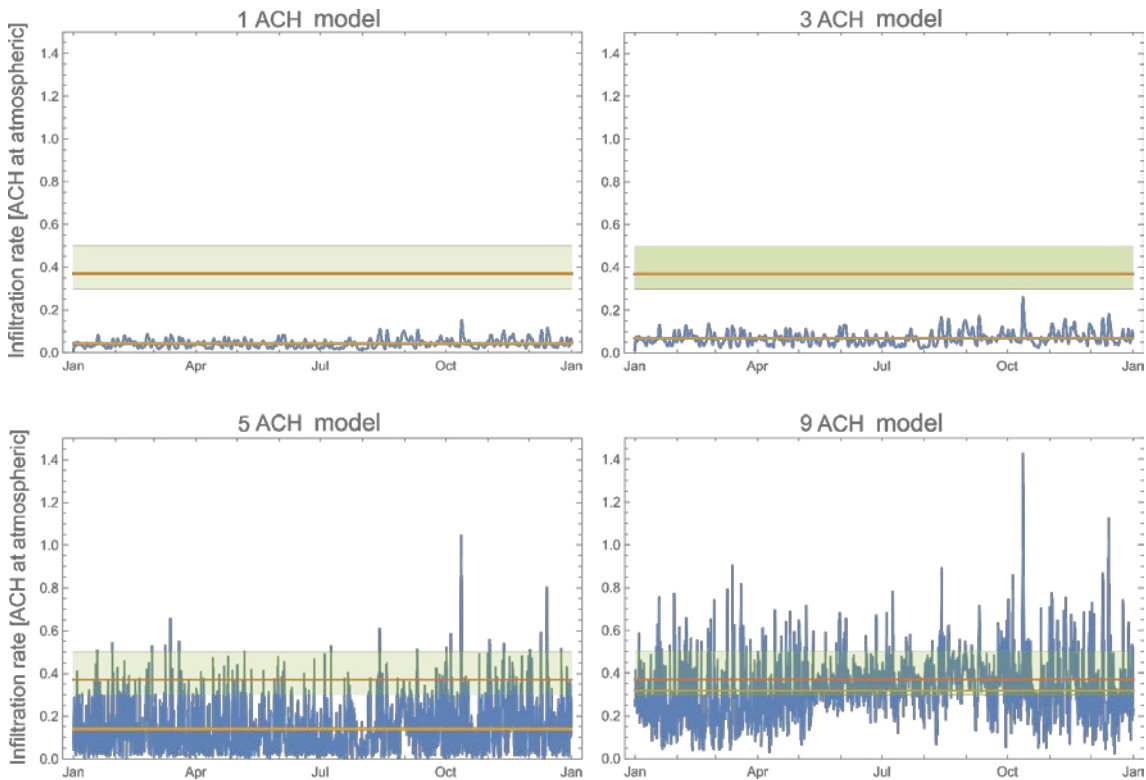


Figure 37. Infiltration model for a single-zone Dunedin house at various airtightness levels.

Summary of results

Table 6. Mean, maximum and minimum infiltration rates at different airtightness levels for different regions around New Zealand. Values were deduced from the models shown above with units given in given in ACH @ atmospheric pressure.

	Northland			Auckland			Taupo			Wellington			Christchurch			Dunedin		
ACH @ 50 Pa	Mean	Max	Min	Mean	Max	Min	Mean	Max	Min	Mean	Max	Min	Mean	Max	Min	Mean	Max	Min
1	0.037	0.13	0.005	0.046	0.14	0.004	0.027	0.10	0.007	0.043	0.13	0.010	0.036	0.10	0.008	0.043	0.15	0.009
3	0.058	0.21	0.008	0.073	0.21	0.007	0.044	0.16	0.012	0.067	0.20	0.017	0.058	0.16	0.016	0.068	0.26	0.014
5	0.12	0.64	0.002	0.15	0.85	0.002	0.086	1.02	0.002	0.13	0.87	0.002	0.12	0.76	0	0.14	1.05	0.002
9	0.23	0.95	0.014	0.27	1.2	0.001	0.26	1.4	0.001	0.27	1.2	0.007	0.31	1.04	0.001	0.32	1.4	0.019

The yearly mean infiltration rate is below the ASHRAE recommended value for acceptable ventilation in all the cities we tested below 9 ACH @ 50 Pa. This result highlights the importance of additional ventilation measures, such as opening windows, in achieving a healthy indoor environment. Table 6 provides a summary of the mean, maximum and minimum infiltration rates for the different regions modelled above.

4.5.3 Two-zone infiltration and ventilation model

The experiments described in section 3.2.6, which are presented in section 4.4, were modelled with the two-zone infiltration and ventilation model described in section 3.2.9. For these experiments, the building was configured as a two-zone system (Figure 9.). Eight models were run in total, and comparisons between the flows calculated in the models and the tracer gas experiments are given below. Figure 38. compares the modelled and measured results where a supply-only ventilator was running at a constant rate in the building. The comparison is of the flows in Zone 2 only. Figure 39. compares the measured and modelled air change rates for the infiltration-only case, again for Zone 2 only. For both figures, the data presented is the mean rate of the dataset, with the error bars representing the standard deviation.

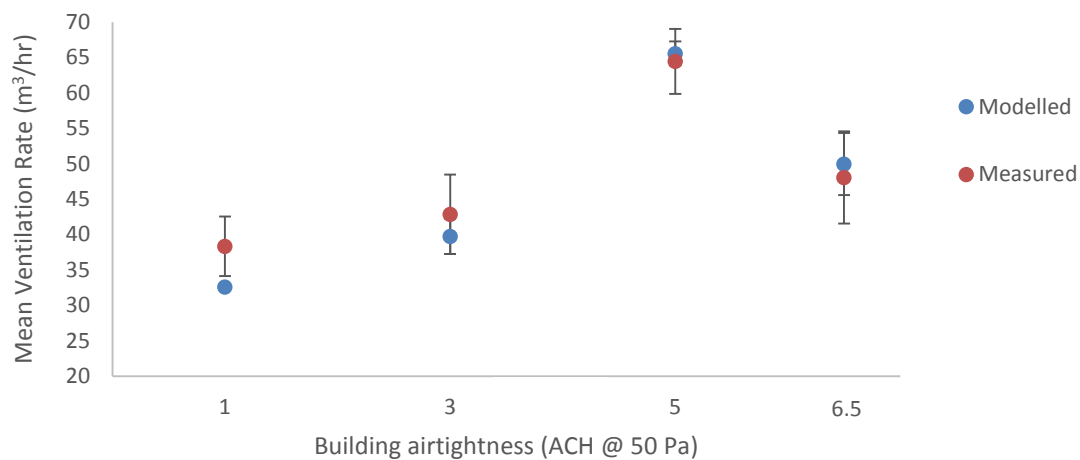


Figure 38. Mean measured and modelled air change rate in Zone 2 over a range of airtightness levels with supply-only ventilation.

Figure 38. show good agreement between measured and modelled data, where the data points and error bars are well within an acceptable range. The higher rate at 5 ACH @ 50 Pa is thought to be due to the wind conditions at the time of the experiment, and the model has captured this well.

Mean air change rate for the two measured and modelled data agree well in Figure 39., with a slight discrepancy at 1 ACH @ 50Pa, where applying the convolution used in section 4.5.1 would yield some improvement. What is evident in Figure 39. is that there is a wider dynamic range in the model compared with the measured data, which is a known limitation of the assumed instant mixing in CONTAM.

The agreement in both sets of models gives confidence that using a two-zone modelling technique in CONTAM will give good agreement to reality. What is crucial, though, is that a building is well categorised in order to estimate the number and size of leakage openings to place in the CONTAM model. This categorisation comes from two sources – an airtightness test and tracer gas experiments.

The models above cover a two-zone building with an airtightness being one of 1, 3, 5 or 6.5 ACH @ 50 Pa and also have the option to supply air at a known rate from the roofspace of the dwelling. This has resulted in a valuable tool for extrapolating the results of contaminant removal effectiveness to different dwelling typologies and climate zones in the country.

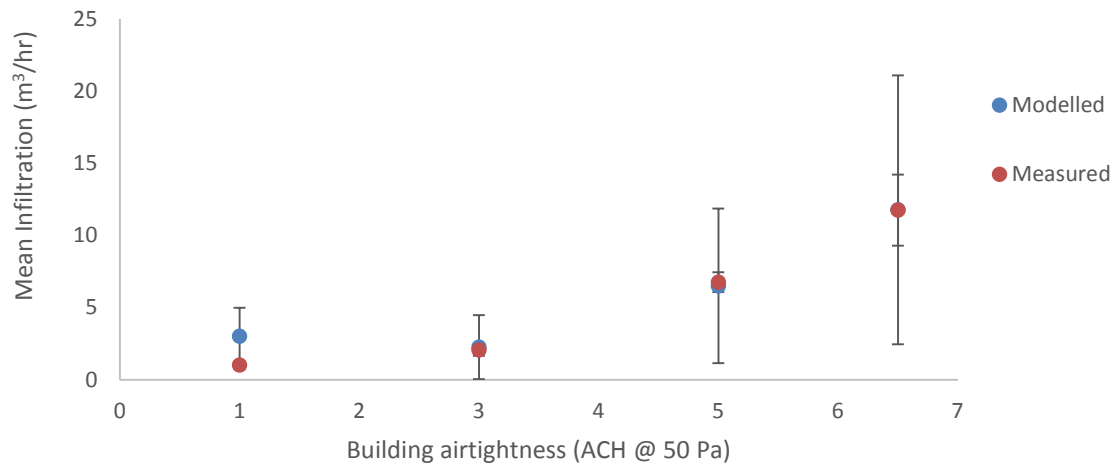


Figure 39. Mean measured and modelled air change rate in Zone 2 over a range of airtightness levels – infiltration only.

4.6 Moisture removal effectiveness

Table 7 presents the results of the moisture removal effectiveness experiments described in section 3.2.7. It presents the mean age of CO₂ (as a proxy for air), the mean age of moisture and the ratio of the two. The mean ages are represented in hours. Experiments were undertaken for four different airtightness configurations, both with and without a supply-only ventilation system running.

Table 7. Mean age of CO₂ and mean age of moisture.

Ventilation configuration	Airtightness [ACH @ 50 Pa]	Mean age CO ₂ [hours]	Mean age moisture [hours]	Relative contaminant removal effectiveness [-]
Infiltration only	9	3.1	11.4	0.27
Infiltration only	5	3.86	11.6	0.33
Infiltration only	3	5.1	11.8	0.43
Infiltration only	1	14.1	12.2	1.16
Supply only	9	1.0	8.9	0.11
Supply only	5	1.0	8.4	0.12
Supply only	3	0.9	9.3	0.10
Supply only	1	1.2	7.7	0.16

In the infiltration-only case, there is a trend to higher mean age of CO₂ as the building becomes more airtight, with little change to the mean age of moisture over the range of airtightness levels studied. The increase in mean age of CO₂ follows the general trend for ventilation rates identified in Figure 23.

The transition from infiltration-only to supply-only ventilation resulted in a large drop in the mean age of CO₂, dropping to about 1 hour. There was little variation in the mean age of CO₂ with airtightness under the positively ventilated regime, where the variation of total ventilation rate was not heavily impacted by the additional infiltration as the airtightness was relaxed. In these cases, the supply-only ventilator dominated the total ventilation rate, with the average ventilation rates being similar for each airtightness level.

The large difference between the infiltration-only and the ventilated case for the mean age of CO₂ is not seen to the same extent for the mean age of moisture. There is some change, dropping from approximately 11.5 hours down to 8.5 hours, but the reduction is certainly not of the same magnitude as the CO₂ case. Interestingly, the mean age of moisture in the supply-only ventilation case suggests a weak upward trend as airtightness is increased. Previous field research of this style of ventilation (Pollard and McNeil, 2010) has shown that, in some cases, the ventilation system could be adding moisture when the absolute moisture content of the roofspace air was higher than that of the dwelling. This could be a contributing factor to this trend, although there is not enough data in this study to confirm this.

Two other factors limit the application of mean age calculation to moisture. Firstly, the buffering of the room is not considered in the mean age calculations, and secondly, incoming air is also likely to be a source of moisture. The modelling results of sections 4.6.1 and 4.6.2 demonstrate that this buffering by materials is still a significant component.

Additional experiments changing the dosing rate of moisture may prove useful in determining the limits of each particular ventilation configuration as the effect of sorption into the building materials changes. There is a clear difference between having mechanical ventilation and having infiltration only.

4.6.1 Rode model

The experiments above indicated a strong dependence on the accumulation of moisture into materials in the room. For this reason, the Rode model (see section 3.2.7.1) was implemented to investigate the contribution of different materials in the room. As the room was unfurnished, this amounted to the absorption by the walls and floors and condensation on the glazing.

Two example plots of the model output versus measured values for the Rode model are shown in Figure 40. and Figure 41., with the time where dosing began marked on the plots with a vertical line. Results are presented as humidity ratio of the air. There is a slight phase shift in the data due to the averaging routine used. The modelled data follows the general trend of the measured data with reasonable agreement. However, the release of some buffered moisture is evident as a second peak just after 6am, which the model does not capture.

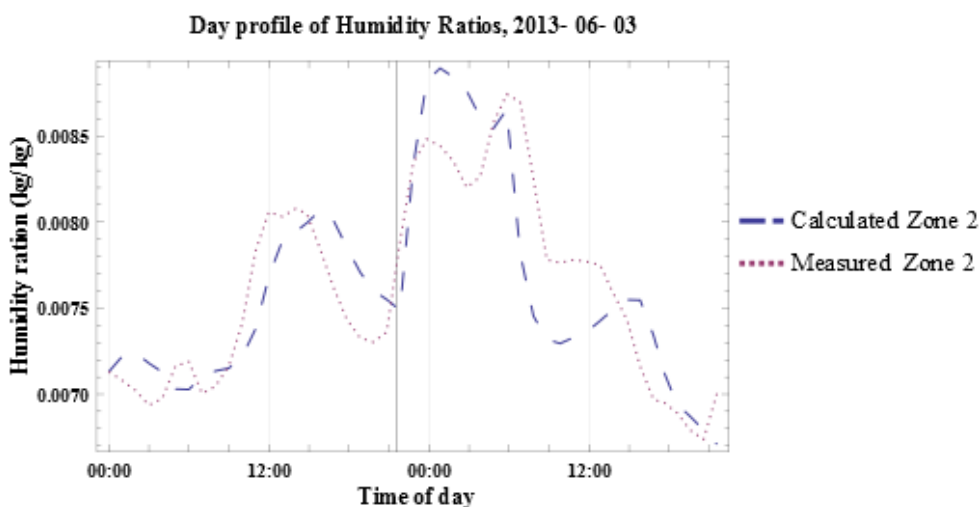


Figure 40. Measured and modelled humidity ratio, 3 ACH @ 50 Pa – supply only.

This peak coincides with switching the heating on in the room, and it is thought that it is condensed water on the glazing evaporating, adding to the measured amount of moisture in the air.

If we calculate the area under the curve for each of the plots in Figure 40. and Figure 41., the differences are quite small – 3.2% for the infiltration-only case and 0.03% for the supply-only ventilation case. In both these cases, the modelled data is slightly underestimated. The agreement between the total areas under the curves indicates that the differences observed looking at the plots are an artefact that can be attributed to sorption/buffering in the room.

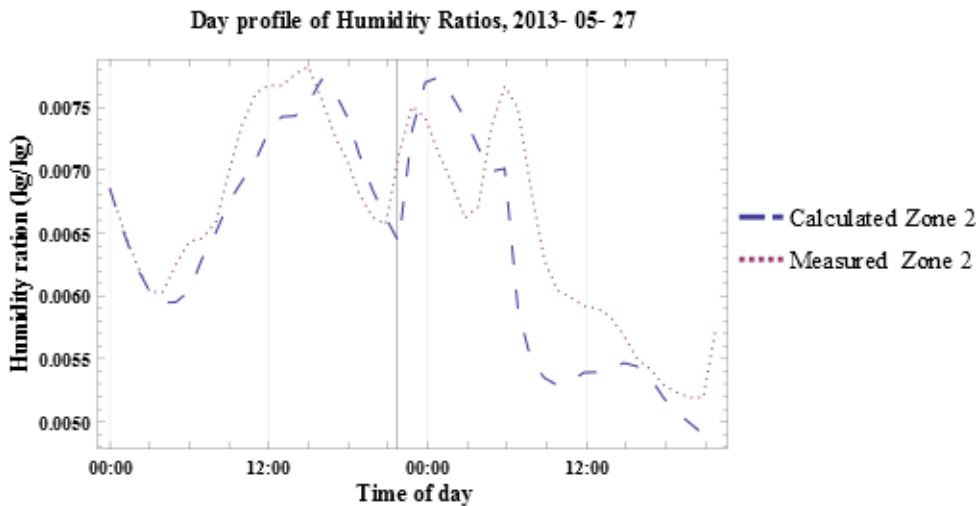


Figure 41. Measured and modelled humidity ratio, 1 ACH @ 50 Pa – infiltration only.

As it stands, the implementation of the Rode model does not have a term for accumulation on the glass. It was decided that, for future work, the ventilation stream of WAVE would adopt the BRANZ nodal model (see section 3.2.7.1). The BRANZ nodal model has a more flexible interface, allowing for the addition of new nodes to represent additional elements, making the process much faster than modifying the Rode model at a very low level each time we want to vary the system under investigation.

The next section describes the results of using the nodal model to understand the experiments in section 3.2.7.

4.6.2 Nodal model

The measurements described in section 3.2.7 on moisture removal effectiveness were modelled with the nodal model described in section 3.2.7.1. In these experiments, the building was configured as a two-zone system in (Figure 9.), where moisture was dosed into the smaller zone (Zone 2) overnight. The dosage rate was equivalent to two sleeping adults. Dosing was switched on in the room for 8 hours/night, starting at 10pm and ending at 6am.

The modelling results are presented in Figure 42 and Figure 43. In both cases, the building was configured to an airtightness of 3 ACH @ 50 Pa, with Figure 42 representing the case where there was no additional ventilation, and Figure 43. where there was a supply-only roofspace-sourced system ventilating at a constant rate. Measured airflows from the experiments were input into the model in order to model the experiments in the greatest detail possible.

Figure 42 compares the measurements in Zone 2 with the output from the nodal model. The measured relative humidity (RH, in red) is compared to the relative humidity as calculated by the model (in blue). The amount of condensation on the node representing the single-glazed windows is plotted in green against a secondary axis.

The agreement between the measured and modelled RH is reasonably good – the mean and standard deviation of the measured data are 94.1% and 5.5%. For the modelled data, these are 87.8% and 9.5%, which does indicate the model appears to be buffering the moisture in the air a little more than reality. The individual moisture dosing periods are evident as the three broad peaks in the two RH curves, starting at approximately 5, 30 and 56 hours.

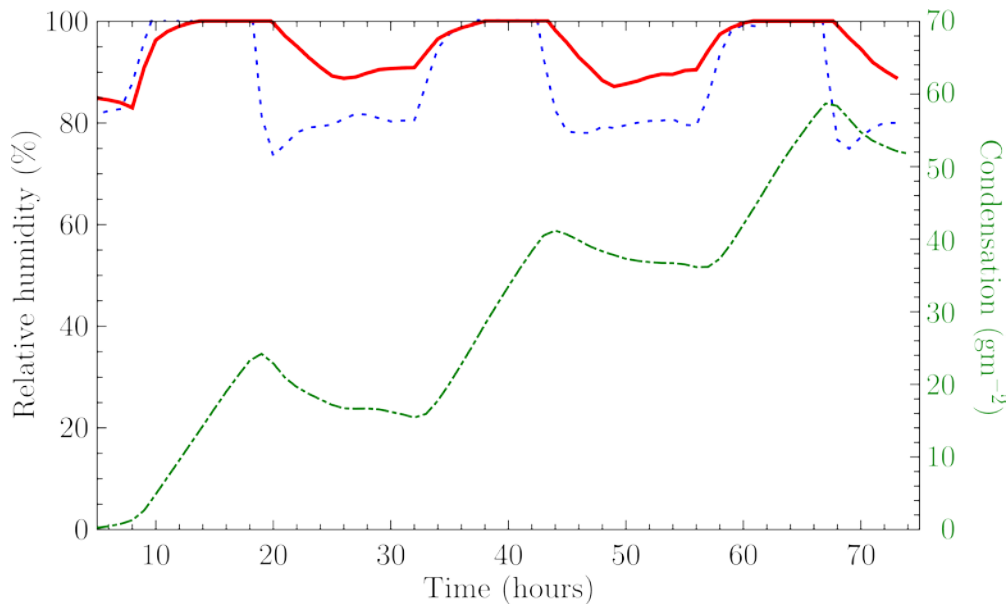


Figure 42. Relative humidity and condensation curves for infiltration-only case. Solid line = measured relative humidity in the centre of the room. Dashed line = model fit of relative humidity. Dash-dot line = amount of condensation on the window given by the right-hand axis.

The node representing the condensation on the glazing is showing an interesting result, which agrees well with what was seen in reality. In effect, the window is not recovering from the moisture dosing the night before. There is a decrease in the amount of condensation for a brief period, but the next dosing event occurs before it is able to dry completely. It is worth noting here that the maximum amount of condensation on the windows in this test building was of the order of 70 gm², which this model is very close to reaching.

Figure 43. show the results from the nodal model for a case similar to the one above but with a supply-only ventilator ventilating the room at a rate of approximately 16 l/s. The plot shows two consecutive nights of moisture dosing, with the dosing events starting at hours 22 and 46. The agreement of the RH between the measured and modelled data is better than the infiltration-only case. In both cases, the mean RH has dropped substantially to 74.6% and 72.3% for the measured and modelled data respectively. Standard deviations are 9.3% and 14.5%. There is a significant difference in the amount of condensation on the glazing for this case. There is still condensation occurring on the glass, but the amount and duration is quite different from the work in Figure 42. This and the change in mean RH are strongly indicative of the effect the additional ventilation is having on the amount of moisture retained in the room.

The level of condensation is only reaching 6 g/m² at worst, which is an order of magnitude less than the infiltration-only case. More important, however, is that the accumulated moisture is evaporating during the day.

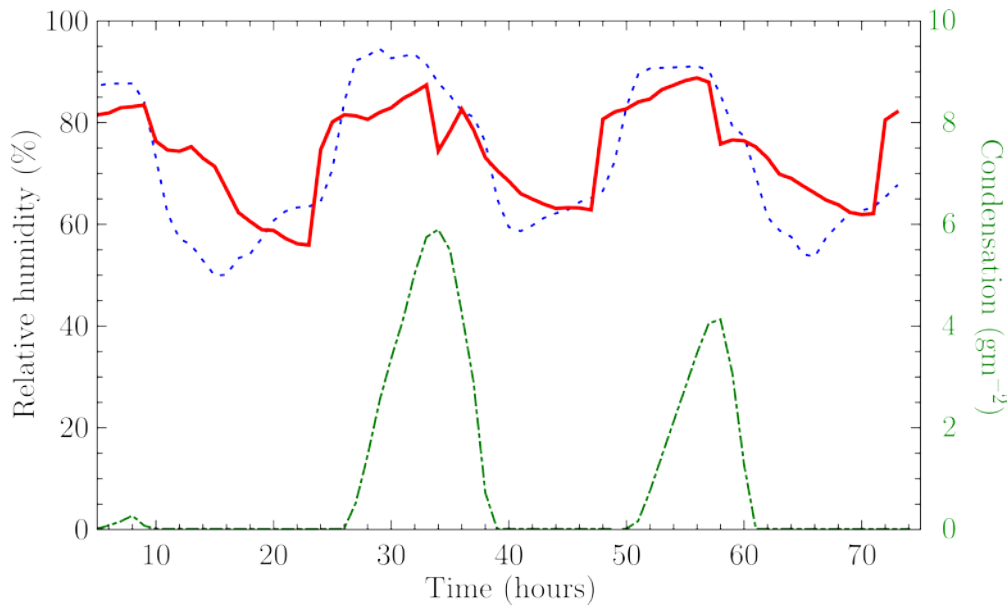


Figure 43. Relative humidity and condensation curves with ventilation system on. Solid line = measured relative humidity in the centre of the room. Dashed line = model fit of relative humidity. Dash-dot line = amount of condensation on the window given by the right-hand axis.

4.7 Control system evaluation

This section presents the results from the moisture flow measurements within two Dunedin homes (labelled DUD 131 and DUD 132) described in section 3.3. The figures and raw data from which conclusions have been drawn here have been published elsewhere in an internal BRANZ publication.

4.7.1 Empirical measurement summary

This analysis focuses on the different patterns of heat and water vapour transfer that occurred in each season. Dunedin has a typical temperate maritime climate with four distinct seasons. For each season, a 5-day period that represents typical weather for that season was chosen. Each period is as near to the solstice or equinox of each season as was feasible to still capture typical weather. Where the 5 days around the solstice or equinox were not representative of that season's typical weather (for instance, it rained heavily for the week around the summer solstice in 2013 while the rest of the summer was comparably dry and warmer), a 5-day period as close as possible to the solstice was used instead. These assessments of typical weather were informed by using measured data at the site and ancillary information.

4.7.2 WUFI Plus modelling summary

To examine moisture flows for DUD 131 and DUD 132, the following parameters output by WUFI Plus were integrated over the period of interest to get the mass (kg) of moisture transferred: moisture exchange with partitions (kg/h); inner moisture source (kg/h); moisture flow due to natural ventilation and infiltration (kg/h); moisture flow due to mechanical ventilation (kg/h); moisture flow due to interzone ventilation (kg/h). The parameters are summarised in Table 8.. Output figures are presented elsewhere as part of an internal BRANZ publication.

Table 8. Parameters output by WUFI Plus model of two Mosgiel-based homes using supply-only ventilation systems.

Parameters	Description
Moisture exchange with partitions (kg/h)	Moisture exchanged with building materials
Inner moisture source (kg/h)	Moisture sourced from within the zone – assumed to be zero in the model runs here
Moisture flow due to natural ventilation and infiltration (kg/h)	Moisture flow through windows, doors, gaps in building structure/materials
Moisture flow due to mechanical ventilation (kg/h)	Moisture flow due to extract fans or other mechanical ventilation – assumed to be zero in the model runs here
Moisture flow due to interzone ventilation (kg/h)	Moisture flow due to the positive-pressure mechanical ventilation system pumping air from the attic to the inside of the house

To examine heat flows, the parameter heat flow interzone ventilation (kW) output by WUFI Plus was integrated over the period of interest to get the net heat flow (kWh). All values greater than zero were integrated to get heat gains (kWh), and all values less than zero were integrated to get heat losses (kWh) due to interzone ventilation under the prototype control algorithm regimes.

4.7.2.1 House DUD 131

There was never a time in July 2013, September 2013 and March 2014 when there was both a temperature benefit and an absolute humidity benefit to pumping roofspace air into the living space. However, there were times during September 2013 and March 2014 (but not July 2013) when there was both a temperature and relative humidity benefit to pumping air from the roofspace into the living space. These facts had important implications for the prototype algorithms:

- The BangBang_QDiff_And_TDiff algorithm (Equation (13)) yielded entirely 0 Ls^{-1} flow rates, and there was no heat and no moisture transfer into the house. This therefore does not seem to be much of a control algorithm, since the system is effectively turned off during those periods. It does, however, suggest that the most effective way to reduce absolute humidity in the house while still maximising heat flow from the roof to indoors is to turn the fan off altogether. This is in direct contrast to some existing control systems where the fan is constantly on, typically at a reduced rate, regardless of temperature difference.
- The BangBang_RHDiff_And_TDiff algorithm (Equation (14)) yielded the most promising results when it gave non-zero flow rates (September 2013 and March 2014). These periods led to minimised heat losses compared to the actual flow rates case (–0.501 kWh and –1.74 kWh, compared to –45.7 kWh and –88.1 kWh). Although the heat gains were less (33.4 kWh and 74.1 kWh, compared to 131 kWh and 118 kWh), net heat gains existed (32.9 kWh and 72.4 kWh, compared to 84.9 kWh and 30.0 kWh). There was also a much smaller moisture transport from the roofspace to the living space (101 kg and 304 kg respectively compared to 895 kg and 1228 kg for actual flow rates case). If the objective of an alternative control algorithm was to minimise unwanted cooling and minimise moisture transport for the roofspace into the living space, this algorithm seems to meet those objectives, at least for the periods studied. However, it should be noted that the net heat gains are not large (at most around 3 kWh per day).
- The BangBang_RHDiff_And_TDiff_with_baseline algorithm (Equation (15)) set a minimum flow rate of 40 Ls^{-1} and then applied higher flow rates when there was

both a temperature and relative humidity benefit to pumping air from the roofspace into the house. The results were similar to those from the actual flow rates but with slightly reduced net heat gains, heat gains, heat losses and moisture transport from the roofspace into the living space. This algorithm did not appear to be a huge improvement on the actual flow rates. It was only ever intended to be a clear comparison with the BangBang_RHDiff_And_TDiff (Equation (14)) to show the impacts due to keeping the low baseline flow rate at all times, which the existing system uses. It appears that the low baseline flow rate in the existing system does not yield a net benefit in terms of heat nor a large reduction in moisture flow compared to the same control strategy without a baseline flow rate.

- The Proportional_QDiff algorithm (Equation (16)) led only to heat losses, because as stated above, there was never a time in July 2013, September 2013 and March 2014 when there was both a temperature benefit and an absolute humidity benefit to pumping roofspace air into the living space. There were very small moisture transport values (2.72 kg, 9.48 kg and 4.51 kg respectively), but overall, this algorithm was not that promising.

4.7.2.2 House DUD 132

Unlike for DUD 131, for DUD 132, the periods 1–23 July 2014, 1–30 September 2013 and 7–31 March 2014 all had times when there was both a temperature benefit and an absolute humidity benefit to pumping roofspace air into the living space. There were also times during all of those periods when there was both a temperature and relative humidity benefit to pumping air from the roofspace into the living space.

- The BangBang_QDiff_And_TDiff algorithm (Equation (13)) yielded non-zero flow rates, and so there was some heat and moisture transfer into the house. This prototype control algorithm resulted in lower net heat gains compared to those from actual flow rates (0.842 kWh, 143 kWh and 113 kWh, compared to 34.5 kWh, 274 kWh and 139 kWh) with lower heat losses (–0.0266 kWh, –0.474 kWh and –3.80 kWh, compared to –17.4 kWh, –23.1 kWh and –46.0 kWh) and lower heat gains (0.869 kWh, 143 kWh and 117 kWh, compared to 51.9 kWh, 298 kWh and 185 kWh). Moisture transfers were also lower (3.98 kg, 329 kg and 396 kg, compared to 402 kg, 957 kg and 942 kg).
- The BangBang_RHDiff_And_TDiff algorithm (Equation (14)) resulted in net heat gains that were lower in July 2014, the same in September 2013 and higher in March 2014 (27.2 kWh, 274 kWh and 261 kWh, compared to 34.5 kWh, 274 kWh and 139 kWh). The heat losses were lower (–0.837 kWh, –2.49 kWh and –10.6 kWh, compared to –17.4 kWh, –23.1 kWh and –46.0 kWh), with heat gains that were lower in July 2014 and September 2013 and higher in March 2014 (28.0 kWh, 277 kWh and 271 kWh, compared to 51.9 kWh, 298 kWh and 185 kWh). Moisture transfers were lower in all three periods (117 kg, 688 kg and 932 kg, compared to 402 kg, 957 kg and 942 kg).
- The BangBang_RHDiff_And_TDiff_with_baseline algorithm (Equation (15)) resulted in net heat gains that were slightly lower, slightly higher and much higher in each period (32.1 kWh, 281 kWh and 241 kWh, compared to 34.5 kWh, 274 kWh and 139 kWh). The heat losses were less (–17.2 kWh, –16.6 kWh and –37.1 kWh, compared to –17.4 kWh, –23.1 kWh and –46.0 kWh) and heat gains slightly lower, the same and much higher (49.2 kWh, 298 kWh and 278 kWh, compared to 51.9 kWh, 298 kWh and 185 kWh). Moisture transfers were less in July 2014 and September 2013 but more in March 2014 (354 kg, 893 kg and 1130 kg, compared to 402 kg, 957 kg and 942 kg).
- The Proportional_QDiff algorithm (Equation (16)) resulted in net heat gains that were much smaller, with losses in July 2014 and March 2014 (–26.2 kWh, 37.1

kWh and -1.11 kWh, compared to 34.5 kWh, 274 kWh and 139 kWh). This result was because both heat losses were larger in all three periods (-40.5 kWh, -29.7 kWh and -53.4 kWh, compared to -17.4 kWh, -23.1 kWh and -46.0 kWh), and heat gains were much lower (14.3 kWh, 66.8 kWh and 52.3 kWh, compared to 51.9 kWh, 298 kWh and 185 kWh). Moisture transfers were lower in all periods (284 kg, 490 kg and 563 kg, compared to 402 kg, 957 kg and 942 kg).

For DUD 132, if the objective of an alternative control algorithm was to minimise unwanted cooling and minimise moisture transport from the roofspace into the living space, none of the algorithms seems to meet those objectives, at least for the periods studied. This is in contrast to the results of DUD 131.

Summary

The very different results for each house could be due to a number of reasons:

- Although both houses are oriented with the main façade facing northwest in both the model and in reality, DUD131 has extensive photovoltaic and solar water heating installed, which could cause shading. DUD132 has no such installations on the roof.
- DUD131 is of older construction than DUD132 and therefore has a higher air changes per hour rate.
- The airtightness of the roofing could be having an effect of retained heat.
- DUD131 has a much smaller fan installed than DUD132 (flow rates around 40 litres per second versus fan rates in excess of 100 litres per second respectively).
- DUD131 has fairly constant measured flow rates, whereas DUD132 has much higher high flow rates and much lower low flow rates.

Table 9. Summary of results for DUD131 and DUD132.

Flow rates		DUD131		DUD132	
		Net heat (kWh)	Interzone moisture transfer (kg)	Net heat (kWh)	Interzone moisture transfer (kg)
July	Actual	49.0	873	34.5	402
	BB_QDiff_TDiff	0	0	0.842	3.98
	BB_RHDiff_TDiff	0	0	27.2	117
	BB_RHDiff_TDiff_baseline	48.5	829	32.1	354
	Prop_QDiff	-0.410	2.72	-26.2	284
	TOTAL DAYS	31 days (2013)		23 days (2014)	
September	Actual	84.9	895	274	957
	BB_QDiff_TDiff	0	0	143	329
	BB_RHDiff_TDiff	72.4	304	274	688
	BB_RHDiff_TDiff_baseline	29.9	1206	281	892
	Prop_QDiff	-1.36	4.51	37.1	490
	TOTAL DAYS	30 days (2013)		30 days (2013)	
March	Actual	30.0	1228	139	942
	BB_QDiff_TDiff	0	0	113	396
	BB_RHDiff_TDiff	32.9	101	261	932
	BB_RHDiff_TDiff_baseline	79.9	835	241	1130
	Prop_QDiff	-5.22	9.48	-1.11	563
	TOTAL DAYS	30 days (2014)		24 days (2014)	

5. Summary

The goal of this study was to investigate the use of ventilation as a means of creating dry, healthy New Zealand homes. Moisture is a well documented problem in many New Zealand houses and is likely to increase as we trend towards more airtight houses without dedicated ventilation systems. We used a combination of empirical data and complex modelling to first highlight the state of ventilation in New Zealand homes and then measure its effectiveness in removing moisture. It is clear from our findings that ventilation is an effective tool for removing moisture and contaminants from the indoor living space. However, infiltration alone is often not enough. Furthermore, our results suggest that the provision for openable windows in clause G4 of the Building Code as the lowest compliance solution for ventilation should be reviewed. With current increasing airtightness trends, it is becoming ever more important to consider ventilation requirements at the design stage of new houses and incorporate them into the structure of the house. There is potential to fall into the trap of continuing to build more airtight, particularly for the purpose of energy efficiency, while ignoring the requirement for adequate ventilation. As we showed in this report, this can lead to increased levels of internal moisture. Since openable windows are the simplest compliance solution for ventilation in new homes, it would be prudent to investigate the role occupant behaviour plays in how often windows are actually opened, as well as other means of ventilation. Future BRANZ research aims to address this question as well as keeping track of current airtightness trends. Key findings from the research described in this report are as follows:

1. A survey of the ventilation and airtightness of 36 houses built after 1994 was conducted. This showed a continued trend of increased airtightness compared to previous surveys of older houses, with the mean airtightness dropping from 8.5 to 6.7 ACH @ 50 Pa. It was also noted that newer houses fell within a smaller range of airtightness levels, indicating more consistent construction. Average ventilation measurements of the same houses taken over 3–4 weeks showed very little change from the background infiltration rate in the majority of houses, suggesting limited window opening during that time.
2. A new test building was constructed for the purpose of this project. The 91 m² building was detailed to have an infiltration of 1 ACH @ 50 Pa. Sealable ports were added in the floor, walls and ceiling such that the airtightness could be varied from 1–13 ACH @ 50 Pa. This allowed us to test different ventilation methods under the same conditions across a range of airtightness levels and provided crucial data to benchmark our models against.
3. We investigated the common assumption that tracer gas is homogeneously mixed with both the air already in the zone and air entering the zone. These experiments were conducted in both the vertical and horizontal plane of a north-facing zone and a south-facing zone. Good mixing was observed in both zones in the vertical plane. However, horizontal mixing in the south-facing zone appears to suffer from stratification during certain parts of the day leading to an uncertainty in infiltration of up to 4%. The underlying driver of poor mixing appeared to be due to a lack of solar radiation creating convections through temperature gradients.
4. At airtightness levels in our test house below 3 ACH @ 50 Pa, a delay between changes in wind velocity and the measured infiltration rate was observed. This effect was not captured in our modelling, as they assume instantaneous, perfect mixing, which was not occurring. We addressed this issue by computationally smoothing the output and convolving it with a response function to imitate what we observed in the empirical data. This was then applied to all our single-zone CONTAM models.

5. A single-zone CONTAM model was created for airtightness levels of 1, 3, 5 and 9 ACH @ 50 Pa and benchmarked against empirical infiltration data from our test house. Using these models and typical mean year (TMY) weather data from NIWA, we modelled the background infiltration rate for different New Zealand cities. Although we only examined six different cities, these models could be used to estimate the infiltration rate of a single-zone building in any part of the country for which TMY data is available. This is useful when determining if extra ventilation (if any) is needed for different houses to effectively manage moisture and other pollutants. Our models showed that infiltration alone is not enough to keep the mean ventilation rate over an entire year within an acceptable range for any of the conditions we examined.
6. We extended our CONTAM model to a two-zone dwelling with an option of including a ventilation system drawing air from the roofspace into the living space. These models were created for infiltration rates of 1, 3, 5 and 6.5 ACH @ 50 Pa and were benchmarked against empirical data taken from our test house. Such models are a valuable tool for estimating the amount of ventilation required for a two-zone building and what effect it might have on contaminant removal. The versatility of these models means they can be used to simulate weather conditions in different parts of the country by importing the appropriate weather files.
7. We measured the mean age of air and moisture in our test house for different airtightness levels both with and without a supply-only ventilation system running. Although there is a distinct decrease in mean age of moisture when the ventilation system is turned on, it is not as pronounced as the decrease in the mean age of air. This phenomenon is due to the moisture-buffering effects of materials inside the house delaying the expulsion of moisture through ventilation. It was also noted, particularly in the infiltration-only case, that infiltration air on the windward side of the building traversed the entire inside of the building before being expelled on the leeward side. This resulted in an increase in the mean age of both air and moisture and highlights the importance of managing moisture at the source and considering the trajectory of air before it is extracted.
8. We developed a nodal model for simulating the mean age of moisture inside a house. This was in response to an earlier model developed by Rode et al. (2001) that we found did not adequately account for condensation forming on glass. Furthermore, our model also captures the moisture-buffering effect we observed in our experiments and has the flexibility to easily add more buffering materials, which the Rode model can not do. We benchmarked our model against empirical data from our test house and showed it to be in excellent agreement.
9. The effectiveness of four different control algorithms for supply-only ventilation systems was compared in situ for temperature, humidity and flow. Two different homes in Mosgiel, Dunedin, were used for this experiment, each yielding quite different results. One home suggested that an algorithm that controlled flow based on relative humidity difference and temperature difference between the roofspace and the living area below was the best method for minimising moisture transport and unwanted cooling. This result, however, was not backed up by the second home. Differences in house design, structure and fan size are attributed with the differing conclusions. What this study did suggest, however, is that determining optimal supply-only ventilation settings is not a trivial task and requires detailed knowledge of the building being considered.

References

- ASHRAE Standard 62.2 (2007). *Ventilation and acceptable indoor air quality in low-rise residential buildings*. American society of heating, refrigerating and air-conditioning engineers inc.
- Barber, E. M. and Ogilvie, J. R. (1984). Incomplete mixing in ventilated airspaces. Part II: Scale model study. *Canadian Agriculture Engineering*, 26 (2), 189–196.
- Bassett, M. R. (1985). The infiltration component of ventilation in New Zealand houses. *Proc. 6th AIC Conference. Ventilation Strategies and Measurement Techniques*, Southern Netherlands.
- Bassett, M. R. with Synergy Applied Research Ltd. (1986). *Survey of air tightness levels in Auckland and Christchurch homes*. New Zealand Energy Research and Development Committee Publication 87.
- Bassett, M. (2000). Pollutant dispersion simulated by a tracer gas in a naturally ventilated test house. *21st AIVC Conference*, The Hague, Netherlands.
- Bassett, M. R. (2001). Naturally ventilated houses in New Zealand simplified air infiltration. *CIB World Building Congress*, Wellington, New Zealand.
- Buckett, N. R., Marston, N. J., Saville-Smith, K., Jowett, J. H. and Jones, M. S. (2011). *Preliminary house condition survey report*. Study Report SR240, BRANZ Ltd, , Judgeford.
- Chao, C. Y., Wan, M. P. and Law, A. K. (2004). Ventilation performance measurement using constant concentration dosing Strategy. *Building and Environment*, 39 (3), 1277–1288.
- Clark, S. J., Jones, M. and Page, I. (2005). *House condition survey*. Study Report SR 142, BRANZ Ltd, Judgeford.
- Department of Building and Housing. (2005a). *Compliance Document for New Zealand Building Code Clause E2 External Moisture*.
- Department of Building and Housing. (2005b). *Compliance Document for New Zealand Building Code Clause G4 Ventilation*.
- Dietz, R. N. and Cote E. A. (1982) Air infiltration measurements in a home using a convenient perfluorocarbon tracer technique. *Environment International*, 8, 419–433.
- EN 13829. (2001). *Thermal performance of buildings. Determination of air permeability of buildings. Fan pressurization method*.
- Haghighat, F., Fazio, P. and Rao, J. (1990). A procedure for measurement of ventilation effectiveness in residential buildings. *Building and Environment*, 25 (2), 163–172.
- Jensen, L. (1986). Determination of leakages in the building envelope using pressurization test measurements. *Air Infiltration Review*, 7 (4), 6–8.
- Liddament, M. W. (1986). *Air infiltration calculation techniques – an applications guide*. Air Infiltration and Ventilation Centre, Berkshire, UK.

- Liddament, M. and Thompson, C. (1983). *Techniques and instrumentation for the measurement of air infiltration in buildings – a brief review and annotated bibliography*. Air Infiltration Centre, Technical Note 10, Berkshire, UK.
- Limb, M. J. (2001). *A review of international ventilation, airtightness, thermal insulation and indoor air quality criteria*. AIVC Document TN55.
- Lunden, M., Faulkner, D., Heredia, E., Cohn, S., Dickeroff, D. J., Noris, F., Louge, J., Toshifumi, H., Singer, B. and Sherman, M. (2012). *Experiments to evaluate and implement passive tracer gas methods to measure ventilation rates in homes*. Lawrence Berkeley Laboratory Report LBNL-5984E.
- Maldonado, E. A. B. and Woods, J. E. (1983). A method to select locations for indoor air quality sampling. *Building and Environment*, 18 (3), 171–180.
- McNeil, S., Plagmann, M. and Bassett, M. (2014). Developing a technique for calculating moisture removal effectiveness in New Zealand homes. *Proc. ICBEST Conference*, Aachen, Germany.
- McNeil, S., Quaglia, L., Bassett, M., Overton, G. and Plagmann, M. (2012). A survey of airtightness and ventilation rates in post 1994 NZ homes. *Proc. 33th AIVC Conference – Optimising ventilative cooling and airtightness for [nearly] zero-energy buildings, IAQ and comfort*, Copenhagen, Denmark.
- Nordtest Method, NT VVS 118: *Ventilation. Local Mean Age of Air – Homogeneous Emission Techniques*.
- Nordtest Method, NT VVS 019: *Buildings – Ventilation Air. Local Mean Age*.
- McDowall, P. D. and Plagmann, M. (2014). Estimating the impact of incomplete tracer gas mixing on infiltration rate measurements. *Proc. 35th AIVC Conference – Ventilation and airtightness in transforming the building stock to high performance*, Poznan, Poland.
- Plathner, P. (2001). *Airborne movement of moisture in dwellings*. PhD Thesis, University of Westminster, London, England.
- Pollard, A. and McNeil, S. (2010). *Forced air ventilation systems*. Report IEQ7570/3 prepared for Beacon Pathway Limited.
- Rode, C., Grau, K. and Mitamura, T. (2001). Model and experiments for hygrothermal conditions of the envelope and indoor air of buildings. *Conference Proceedings of Performance of Exterior Envelope of Whole Buildings VIII*, Clearwater Beach, USA.
- Rudd, A., Lstiburek, J. and Townsend, A. (2009). A calibrated multi-zone airflow model for extension of ventilation system tracer gas testing. *ASHRAE Transactions*, 115 (2).
- Sandberg, M. (1983). Ventilation efficiency as a guide to design. *ASHRAE Transactions*, 89 (2B).
- Sandberg, M. and Stymne, H. (1989). The constant tracer flow technique. *Building and Environment*, 24 (3), 209–219.

- Shao, L. and Riffat, S. B. (1994). Tracer-gas mixing with air: effect of tracer species. *Applied Energy*, 49, 197–211.
- Sherman, M. H. (1990). Tracer-gas techniques for measuring ventilation in a single zone. *Building and Environment*, 24 (4), 365–374.
- Sherman, M. (1998). *Air infiltration measurement techniques*. Revision of Lawrence Berkeley Laboratory publication LBL-10705.
- Sherman, M. H. and Chan, R. (2003). *Building airtightness: research and practice*. Lawrence Berkeley Laboratory report LBNL-53356.
- Sherman, M. H., Walker, I. S. and Lunden, M. M. (2014). Uncertainties in air exchange using continuous-injection long-term sampling tracer-gas methods. *International Journal of Ventilation*, 13 (1), 13–27.
- Stephen R. K. (1998). *Airtightness in UK dwellings: BRE's test results and their significance*. Building Research Establishment Report 359, United Kingdom.
- Trethowen, H. A. (1972). *Dampness in housing*. Report CR2, Building Research Association of New Zealand.
- Upton, S. and Kukadia, V. (2011). *Ventilation rate measurement*. BRE Information Paper IP 13/1. ISBN 978-1-84806-219-1Pla.
- Van Buggenhout, S., Van Brecht, A., Eren Özcan, S., Vranken, E., Van Malcot, W. and Berckmans, D. (2009). Influence of sampling positions on accuracy of tracer gas measurements in ventilated spaces. *Biosystems Engineering*, 104, 216–223.